Synthetic Modeling of Nitrite Binding and Activation by Reduced Copper Proteins. Characterization of Copper(I)−Nitrite Complexes That Evolve Nitric Oxide

Jason A. Halfen, Samiran Mahapatra, Elizabeth C. Wilkinson, Alan J. Gengenbach, Victor G. Young, Jr., Lawrence Que, Jr., and William B. Tolman*

Contribution from the Department of Chemistry, University of Minnesota, 207 Pleasant Street S. E., Minneapolis, Minnesota 55455

Received August 8, 1995[⊗]

Abstract: In an effort to provide precedence for postulated intermediates in copper-protein-mediated nitrite reduction, a series of novel complexes containing the $Cu^{I}-NO_2^-$ unit, including monocopper(I), dicopper(I,I), and mixed valence dicopper(I,II) and copper(I)−zinc(II) species, were prepared, fully characterized, and subjected to reactivity studies designed to probe their ability to produce nitric oxide. Treatment of solutions of $[LCu(CH_3CN)]PF_6$ (L = $L^{i\text{-}Pr_3}$, 1,4,7-triisopropyl-1,4,7-triazacyclononane, or L^{Bn_3}, 1,4,7-tribenzyl-1,4,7-triazacyclononane) in MeOH with excess $NaNO_2$ yielded the novel dicopper(I,I) complexes $[(LCu)_2(\mu\text{-}NO_2)]PF_6$. The complex with L = $L^{i\text{-}Pr_3}$ was cleaved by PPh_3 to afford $[L^{i\text{-}Pr_3}Cu(PPh_3)]PF_6$ and $L^{i\text{-}Pr_3}Cu(NO_2)$, a structural model for the substrate adduct of copper nitrite reductase. Oxidation of the dicopper(I,I) compound (L = $L^{i\text{-}Pr_3}$) with $(Cp_2Fe)(PF_6)$ in CH_2Cl_2 yielded the deep red, mixed valent, dicopper(I,II) species $[(L^{i\text{-}Pr_3}Cu)_2(\mu\text{-}NO_2)](PF_6)_2$, which was structurally characterized as its $[B(3,5\text{-}(CF_3)_2C_6H_3)_4]^-$ salt (crystal data: triclinic space group $P\bar{1}$, a = 13.439(8) Å, b = 13.777(5) Å, c = 14.471(8) Å, α = 108.22(4)°, β = 92.08(5)°, γ = 90.08(4)°, Z = 1, T = 177 K, R = 0.074, and R_w = 0.070). A diamagnetic heterodinuclear $Cu^{I}Zn^{II}$ analog, $[L^{i\text{-}Pr_3}Cu(\mu\text{-}NO_2)ZnL^{i\text{-}Pr_3}](O_3SCF_3)_2$, was assembled by mixing $L^{i\text{-}Pr_3}Cu(NO_2)$, $Zn(O_3SCF_3)_2$, and $L^{i\text{-}Pr_3}$ and was shown to adopt a structure similar to that of its $Cu^{I}Cu^{II}$ relative (crystal data: monoclinic space group $P2_1/c$, a = 10.8752(1) Å, b = 15.6121(3) Å, c = 25.8020(5) Å, β = 90.094(1)°, Z = 4, $R1$ = 0.0472, and w$R2$ = 0.1082). Both compounds exhibit an intense electronic absorption feature that was assigned as a $Cu^{I} \rightarrow NO_2^-$ MLCT transition on the basis of resonance Raman spectroscopic results. Functional modeling of copper nitrite reductase was accomplished by treating solutions of $L^{i\text{-}Pr_3}Cu(NO_2)$ with protonic acids or $Me_3SiO_3SCF_3$. Nitric oxide evolution was accompanied by the formation of $L^{i\text{-}Pr_3}Cu(O_2CCH_3)_2$ and $L^{i\text{-}Pr_3}Cu(O_3SCF_3)_2$ when acetic acid or $Me_3SiO_3SCF_3$ was used. The latter crystallized as a water adduct $[L^{i\text{-}Pr_3}Cu(H_2O)(O_3SCF_3)](O_3SCF_3)$ (crystal data: monoclinic space group $P2_1/c$, a = 8.59(1) Å, b = 26.04(1) Å, c = 12.838(4) Å, β = 108.26(6)°, Z = 4, T = 173 K, R = 0.067, and R_w = 0.064). The involvement of the $Cu^{I}Cu^{II}$ species as an intermediate in the reaction of $L^{i\text{-}Pr_3}Cu(NO_2)$ with $Me_3SiO_3SCF_3$ at low temperature and a mechanism for NO generation involving both $L^{i\text{-}Pr_3}Cu(NO_2)$ and $[(L^{i\text{-}Pr_3}Cu)_2(\mu\text{-}NO_2)]^{2+}$ are discussed.

Denitrification, the dissimilatory, enzymatic reduction of nitrate (NO_3^-) and nitrite (NO_2^-) to gaseous NO, N_2O, and/or N_2, is a key process in the global nitrogen cycle whereby simple organisms utilize the oxidizing equivalents of nitrogen oxides to drive metabolic processes.[1] The environmental consequences of denitrification are profound, as it is responsible for the degradation of the agriculturally useful yet polluting nitrogen oxides NO_3^- and NO_2^- and for the generation of the reactive gaseous molecules NO and N_2O that are implicated in ozone depletion, atmospheric warming, and air pollution.[2] These environmental issues, coupled with the recently realized importance of nitrogen oxide chemistry in mammalian systems,[3] have provided considerable stimulus for research into the properties of the enzymes responsible for NO_x reduction.

The copper-containing nitrite reductases (NiRs) isolated from bacteria[1,4] and, more recently, from fungi[5] comprise an important subclass of the set of denitrification enzymes. Copper NiRs catalyze the reduction of NO_2^- to NO, although N_2O generation has been induced under some conditions.[6] The active site of the copper NiR from *Achromobacter cycloclastes* has been shown by X-ray crystallography[4,7,8] to contain a pair of copper ions (Figure 1), one of which (Cu-I) has been assigned as a "green" type 1, electron transfer site on the basis of its typical $(His)_2(Cys)(Met)$ donor set and its combined electronic absorption [λ_{max} 458 (ϵ 2530), 585 (ϵ 1890) nm], EPR (axial, $A_{||} = 69 \times 10^{-4}$ cm^{-1}), and resonance Raman [multiple Cu−S(Cys) modes between 250 and 500 cm^{-1}] spectroscopic properties.[9,10]

* Author to whom correspondence should be addressed.

[⊗] Abstract published in *Advance ACS Abstracts,* January 1, 1996.

(1) (a) Kroneck, P. M. H.; Beuerle, J.; Schumacher, W. In *Degradation of Environmental Pollutants by Microorganisms and their Metalloenzymes*; Sigel, H., Sigel, A., Eds.; Marcel Dekker: New York, 1992; Vol. 28, pp 455−505.

(2) *Denitrification, Nitrification, and Atmospheric Nitrous Oxide*; Delwiche, C. C., Ed.; John Wiley & Sons: New York, 1981.

(3) *The Biology of Nitric Oxide*; Moncada, S., Marletta, M. A., Hibbs, J. B., Higgs, E. A., Eds.; Portland Press: London, 1992; Vols. 1 and 2.

(4) Adman, E. T.; Turley, S. K. In *Bioinorganic Chemistry of Copper*; Karlin, K. D., Tyeklár, Z., Eds.; Chapman & Hall, Inc.: New York, 1993; pp 397−405.

(5) Kobayashi, M.; Shoun, H. *J. Biol. Chem.* **1995**, *270*, 4146−4151.

(6) Jackson, M. A.; Tiedje, J. M.; Averill, B. A. *FEBS Lett.* **1991**, *291*, 41−44.

(7) Godden, J. W.; Turley, S.; Teller, D. C.; Adman, E. T.; Liu, M. Y.; Payne, W. J.; LeGall, J. *Science* **1991**, *253*, 438−442.

(8) A similar structure has been deduced for the enzyme from *Alcaligenes faecalis* S-6: Kukimoto, M.; Nishiyama, M.; Murphy, M. E. P.; Turley, S.; Adman, E. T.; Horinouchi, S.; Beppu, T. *Biochemistry* **1994**, *33*, 5346−5252.

0002-7863/96/1518-0763$12.00/0

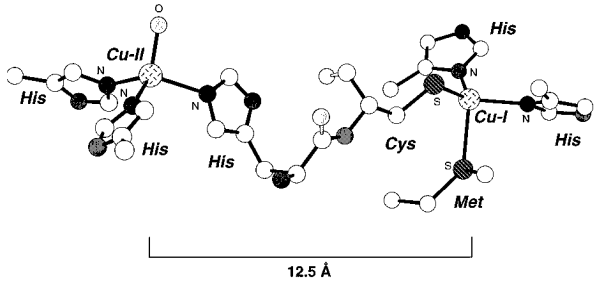

Figure 1. Chem3D view of the active site of nitrite reductase (NiR) from *Achromobacter cycloclastes* (generated from pdb 1afn.full).

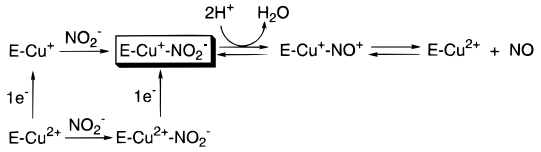

Figure 2. Proposed mechanism for nitrite reduction by NiR.

The other site (Cu-II), which is linked to Cu-I via a dipeptide fragment (Cys136-His135; Cu-I···Cu-II = 12.5 Å), is an unusual, distorted type 2 site, in which the copper ion is bound at the interface between subunits of the trimeric protein by a facial array of three histidine residues. A fourth ligand, refined as a water molecule in the crystallographic analysis,[4,7] completes the pseudotetrahedral environment about this copper site.

On the basis of the crystallographic analysis of nitrite-soaked NiR,[4,7] activity studies on type 2 depleted enzyme,[11] EPR and ENDOR data for the related copper NiR from *Alcaligenes xylosoxidans*,[12] effects of site-directed mutagenesis of copper ligands,[8] and pulse radiolysis experiments interpreted to support intramolecular electron transfer,[13] Cu-II has been suggested to be the locus for nitrite binding and subsequent activation, with Cu-I acting to shuttle electrons, perhaps via the Cys-His bridge, during catalysis. Drawing an analogy to mechanisms deduced for the more thoroughly studied iron heme-containing NiRs for which numerous synthetic models exist,[14] Averill and co-workers proposed that a nitrite adduct to Cu-II in its reduced state [i.e., a $Cu^{I}-NO_2^-$ complex] is a key reaction intermediate (Figure 2).[6,11,15] This intermediate may be envisioned to form via reduction of a $Cu^{II}-NO_2^-$ precursor or directly, via substrate binding to the prereduced Cu^{I} site. Subsequent dehydration to yield an electrophilic copper−nitrosyl (originally written as $Cu^{I}-NO^+$)[14a] followed by release of NO, the principal enzyme product, is then postulated to generate the oxidized Cu-II center ready for reentry into the catalytic process.

Although reasonable, the sequence depicted in Figure 2 had little firm precedent in copper coordination chemistry at the outset of the present work.[16,17] In particular, while several mononuclear $Cu^{II}-NO_2^-$ complexes with biomimetic ancillary ligands had been described,[17b,18] there existed no example of a $Cu^{I}-NO_2^-$ complex in the literature. In view of its potentially central role in the enzymatic nitrite reduction pathway, we targeted such a species for synthetic, structural, spectroscopic, and reactivity studies. Controversy surrounding the existence of $Cu^{I}-NO_2^-$ interactions in copper proteins other than NiR provided further rationale for synthetic modeling,[19] putative nitrite adducts of hemocyanin being noteworthy in this regard.[20] Herein we report details of the synthesis and full characterization of a series of novel biomimetic complexes containing the $Cu^{I}-NO_2^-$ moiety supported by sterically hindered triazacyclononanes, including monocopper(I), dicopper(I,I), and mixed valence dicopper(I,II) and copper(I)−zinc(II) species. We also report reactivity and mechanistic studies that demonstrate the feasibility of key aspects of the pathway shown in Figure 2. Portions of this work were communicated previously.[21]

Results and Discussion

Syntheses. Reference to the crystallographic data for copper NiR suggested that use of a ligand(s) that would provide three nitrogen donor atoms disposed in a facially-coordinating array and that would enforce a pseudotetrahedral copper ion geometry would be a prerequisite for accurate modeling of the Cu-II catalytic site. Our previous successful preparations of copper(II)−nitrite[17b] and copper(I)−nitrosyl[17a] adducts supported by sterically hindered tris(pyrazolyl) hydroborates ($Tp^{RR'}$, where R and R′ are substituents at the 3- and 5-pyrazolyl positions, respectively)[22] suggested that such ligands might also allow the synthesis of the desired $Cu^{I}-NO_2^-$ species. This strategy was not successful, however, despite numerous attempts either to

(9) (a) Lu, Y.; LaCroix, L. B.; Lowery, M. D.; Solomon, E. I.; Bender, C. J.; Peisach, J.; Roe, J. A.; Gralla, E. B.; Valentine, J. S. *J. Am. Chem. Soc.* **1993**, *115*, 5907−5918 and references cited therein. (b) Han, J.; Loehr, T. M.; Lu, Y.; Valentine, J. S.; Averill, B. A.; Sanders-Loehr, J. *J. Am. Chem. Soc.* **1993**, *115*, 4256−4263. (c) Andrew, C. R.; Yeom, H.; Valentine, J. S.; Karlsson, B. G.; Bonander, N.; van Pouderoyen, G.; Canters, G. W.; Loehr, T. M.; Sanders-Loehr, J. *J. Am. Chem. Soc.* **1994**, *116*, 11489−11498.

(10) Abraham, Z. H. L.; Lowe, D. J.; Smith, B. E. *Biochem. J.* **1993**, *295*, 587−593.

(11) Libby, E.; Averill, B. A. *Biochem. Biophys. Res. Commun.* **1992**, *187*, 1529−1535.

(12) Howes, B. D.; Abraham, Z. H. L.; Lowe, D. J.; Bruser, T.; Eady, R. R.; Smith, B. E. *Biochemistry* **1994**, *33*, 3171−3177.

(13) Suzuki, S.; Kohzuma, T.; Deligeer; Yamaguchi, K.; Nakamura, N.; Shidara, S.; Kobayashi, K.; Tagawa, S. *J. Am. Chem. Soc.* **1994**, *116*, 11145−11146.

(14) (a) Weeg-Aerssens, E.; Tiedje, J. M.; Averill, B. A. *J. Am. Chem. Soc.* **1988**, *110*, 6851−6856. (b) Garber, E. A. E.; Hollocher, T. C. *J. Biol. Chem.* **1982**, *257*, 8091−8097. (c) Fanning, J. C. *Coord. Chem. Rev.* **1991**, *110*, 235−273 and references cited therein.

(15) (a) Hulse, C. L.; Averill, B. A.; Tiedje, J. M. *J. Am. Chem. Soc.* **1989**, *111*, 2322−2323. (b) Ye, R. W.; Toro-Suarez, I.; Tiedje, J. M.; Averill, B. A. *J. Biol. Chem.* **1991**, *266*, 12848−12851.

(16) (a) Paul, P. P.; Tyeklár, Z.; Farooq, A.; Karlin, K. D.; Liu, S.; Zubieta, J. *J. Am. Chem. Soc.* **1990**, *112*, 2430−2432. (b) Paul, P. P.; Karlin, K. D. *J. Am. Chem. Soc.* **1991**, *113*, 6331−6332.

(17) (a) Ruggiero, C. E.; Carrier, S. M.; Antholine, W. E.; Whittaker, J. W.; Cramer, C. J.; Tolman, W. B. *J. Am. Chem. Soc.* **1993**, *115*, 11285−11298. (b) Ruggiero, C. E.; Carrier, S. M.; Tolman, W. B. *Angew. Chem., Int. Ed. Engl.* **1993**, *33*, 895−897.

(18) (a) Jiang, F.; Conry, R. R.; Bubacco, L.; Tyeklár, Z.; Jacobson, R. R.; Karlin, K. D.; Peisach, J. *J. Am. Chem. Soc.* **1993**, *115*, 2093−2102. (b) Tolman, W. B. *Inorg. Chem.* **1991**, *30*, 4878−4880 and references cited therein. (c) Komeda, N.; Nagao, H.; Adachi, G.; Suzuki, M.; Uehara, A.; Tanaka, K. *Chem. Lett.* **1993**, 1521−1524. (d) Komeda, N.; Nagao, H.; Kushi, Y.; Adachi, G.; Suzuki, M.; Uehara, A.; Tanaka, K. *Bull. Chem. Soc. Jpn.* **1995**, *68*, 581−589.

(19) (a) Spira, D. J.; Solomon, E. I. *Biochem. Biophys. Res. Commun.* **1983**, *112*, 729−736. (b) Schoot Uiterkamp, A. J. M. S.; van der Deen, H.; Berendsen, H. C. J.; Boas, J. F. *Biochim. Biophys. Acta* **1974**, *372*, 407−425.

(20) (a) van der Deen, H.; Hoving, H. *Biochemistry* **1977**, *16*, 3519−3525. (b) Himmelwright, R. S.; Eickman, N. C.; Solomon, E. I. *Biochem. Biophys. Res. Commun.* **1978**, *81*, 237−242. (c) Himmelwright, R. S.; Eickman, N. C.; Solomon, E. I. *Biochem. Biophys. Res. Commun.* **1979**, *86*, 628−634. (d) Himmelwright, R. S.; Eickman, N. C.; Solomon, E. I. *J. Am. Chem. Soc.* **1979**, *101*, 1576−1586. (e) Verplaetse, J.; Tornout, P. V.; Degreyn, G.; Witters, R.; Lontie, R. *Eur. J. Biochem.* **1979**, *95*, 327−331. (f) Tahon, J.-P.; Hoof, D. V.; Vinckier, C.; Witters, R.; de Ley, M.; Lontie, R. *Biochem. J.* **1988**, *249*, 891−896. (g) Salvato, B.; Giacometti, G. M.; Beltramini, M.; Zilio, F.; Giacometti, G.; Magliozzo, R. S.; Peisach, J. *Biochemistry* **1989**, *28*, 680−84. (h) Magliozzo, R. S.; Bubacco, L.; McCracken, J.; Jiang, F.; Beltramini, M.; Salvato, B.; Peisach, J. *Biochemistry* **1995**, *34*, 1513−1523. (i) Bubacco, L.; Magliozzo, R. S.; Wirt, M. D.; Beltramini, M.; Salvato, B.; Peisach, J. *Biochemistry* **1995**, *34*, 1524−1533.

(21) (a) Halfen, J. A.; Mahapatra, S.; Olmstead, M. M.; Tolman, W. B. *J. Am. Chem. Soc.* **1994**, *116*, 2173−2174. (b) Halfen, J. A.; Tolman, W. B. *J. Am. Chem. Soc.* **1994**, *116*, 5475−5476.

(22) (a) Trofimenko, S. *Chem. Rev.* **1993**, *93*, 943−980. (b) Kitajima, N.; Tolman, W. B. *Prog. Inorg. Chem.* **1995**, *43*, 419−531. (c) Parkin, G. *Adv. Inorg. Chem.* **1995**, *42*, 291−393.

Scheme 1

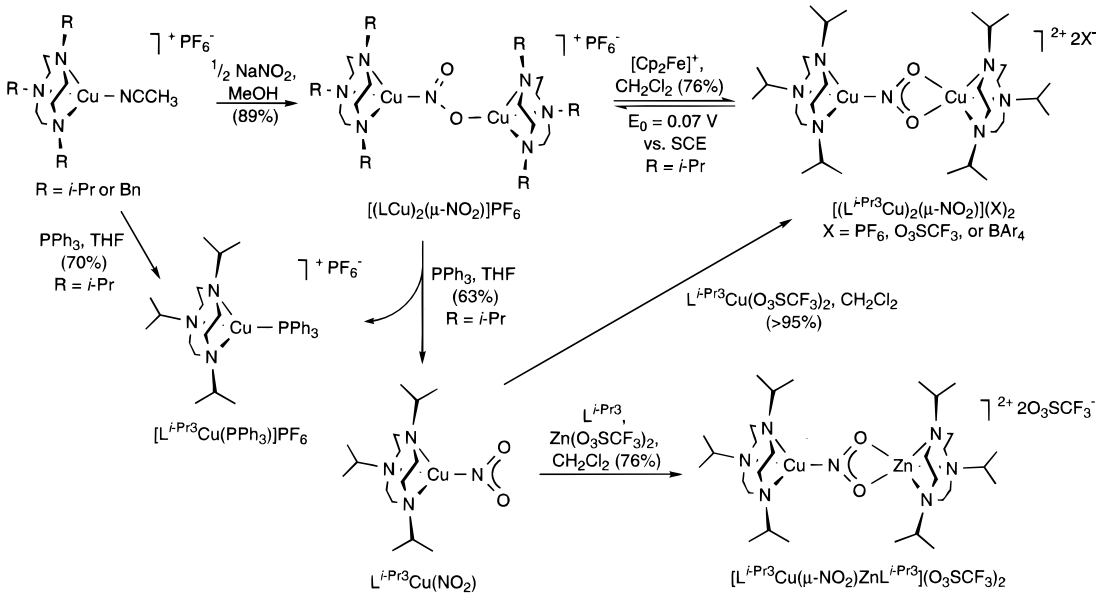

add nitrite salts to $Tp^{RR'}Cu^{I}$ compounds[23] or to reduce preformed $Tp^{RR'}Cu^{II}-NO_2^-$ complexes.[17b,18b] Reasoning that nitrite coordination to a $Tp^{RR'}Cu^{I}$ fragment might be disfavored in the nonpolar solvents most amenable for the handling of hindered $Tp^{RR'}$ complexes because of charge considerations ($Tp^{RR'}$ is a monoanion, making the copper(I) fragment neutral and a derived nitrite adduct anionic), we turned to the sterically hindered, neutral macrocycles 1,4,7-triisopropyl-1,4,7-triazacyclononane ($L^{i\text{-}Pr_3}$)[24] and 1,4,7-tribenzyl-1,4,7-triazacyclononane (L^{Bn_3})[25] recently reported by Wieghardt and co-workers. The trialkyl substituents borne by these molecules render them and their complexes soluble in many organic solvents and prevent deleterious bis(ligand) complex (L_2Cu) formation, as seen with the unsubstituted 1,4,7-triazacyclononane.[26] Although a variety of copper(II) complexes have been prepared with triazacyclononanes,[27] few examples of copper(I) complexes of these ligands existed at the outset of our work.[28]

Stirring $L^{i\text{-}Pr_3}$ or L^{Bn_3} with $[Cu(CH_3CN)_4]PF_6$ in THF generated the highly air and water sensitive copper(I) complexes $[LCu(CH_3CN)]PF_6$ ($L = L^{i\text{-}Pr_3}$ or L^{Bn_3}), which were isolated as solids and characterized by elemental analysis and FTIR and NMR spectroscopy (Scheme 1). Because of concerns that protic solvents might react with nitrite adducts of these starting materials, we initially attempted to synthesize such species by treating $[LCu(CH_3CN)]PF_6$ with soluble $(PPN)(NO_2)$[29] in CH_3CN. However, only slow evolution of NO (1 equiv by GC analysis of the reaction head space) and gradual development of a green, presumably copper(II)-containing solution was observed. In contrast, when excess $NaNO_2$ was added to solutions of $[LCu(CH_3CN)]PF_6$ in MeOH, the dicopper(I,I) complexes $[(LCu)_2(\mu\text{-}NO_2)]PF_6$ ($L = L^{i\text{-}Pr_3}$ or L^{Bn_3}) were isolated as a yellow crystalline solids in high yield (Scheme 1). These products were characterized by analytical, spectroscopic, and, for the complex containing $L^{i\text{-}Pr_3}$, X-ray crystallographic methods. No evidence for the formation of mononuclear complexes was found (^1H NMR), even though excess $NaNO_2$ was used in the synthesis. Nonetheless, regioselective cleavage of $[(L^{i\text{-}Pr_3}Cu)_2(\mu\text{-}NO_2)]PF_6$ was effected by adding 1 equiv of PPh_3, affording analytically pure $[L^{i\text{-}Pr_3}Cu(PPh_3)]PF_6$ and $L^{i\text{-}Pr_3}Cu(NO_2)$ in 97% and 63% yields, respectively, after fractional crystallization. Identification of $L^{i\text{-}Pr_3}Cu(NO_2)$ as the first example of a mononuclear copper(I)−nitrite complex was confirmed by X-ray crystallography. Coproduct $[L^{i\text{-}Pr_3}Cu(PPh_3)]PF_6$ was identified by comparison of its spectroscopic properties to material synthesized independently via the reaction of $[L^{i\text{-}Pr_3}Cu(CH_3CN)]PF_6$ with PPh_3.

The observation of a chemically reversible one-electron oxidation in the cyclic voltammogram of $[(L^{i\text{-}Pr_3}Cu)_2(\mu\text{-}NO_2)]PF_6$ ($E_{1/2} = 0.07$ V vs SCE in CH_2Cl_2; see below) indicated that isolation of a mixed valence nitrite-containing complex would be possible. Indeed, addition of $(Cp_2Fe)(PF_6)$ to $[(L^{i\text{-}Pr_3}Cu)_2(\mu\text{-}NO_2)]PF_6$ in CH_2Cl_2 afforded the deep red crystalline dicopper(I,II) complex $[(L^{i\text{-}Pr_3}Cu)_2(\mu\text{-}NO_2)](PF_6)_2$ (Scheme 1), which was characterized by analytical and spectroscopic methods. We were unable to elucidate the structure of this compound or its $CF_3SO_3^-$ salt via X-ray crystallography due to extensive disorder problems, and attempts to obtain the material with BPh_4^- as counterion failed because of decomposition of the complex via an apparent redox reaction(s) [bleaching of color indicative of the formation of copper(I) species]. However, metathesis with the more redox inert $Na[B(3,5\text{-}(CF_3)_2C_6H_3)_4]$[30] in CH_2Cl_2 was successful and the resulting crystalline product proved to be amenable to crystallographic analysis. The dicopper(I,I) complex of L^{Bn_3}, $[(L^{Bn_3}Cu)_2(\mu\text{-}NO_2)]PF_6$, was less well-behaved electrochemically (irreversible oxidation at $E_{pa} = 0.41$ V vs SCE in CH_2Cl_2), and attempts to prepare a mixed valuence complex via oxidation with $(Cp_2Fe)(PF_6)$ or (NO)-

(23) Carrier, S. M.; Ruggiero, C. E.; Houser, R. P.; Tolman, W. B. *Inorg. Chem.* **1993**, *32*, 4889−4899 and references cited therein.

(24) Haselhorst, G.; Stoetzel, S.; Strassburger, A.; Walz, W.; Wieghardt, K.; Nuber, B. *J. Chem. Soc., Dalton Trans.* **1993**, 83−90.

(25) Beissel, T.; Vedova, B. S. P. C. D.; Wieghardt, K.; Boese, R. *Inorg. Chem.* **1990**, *29*, 1736−1741.

(26) Nonoyama, M. *Trans. Met. Chem.* **1976**, *1*, 70−74.

(27) (a) Wieghardt, K.; Chaudhuri, P. *Prog. Inorg. Chem.* **1988**, *35*, 329−436 and references cited therein. (b) Chaudhuri, P.; Oder, K. *J. Chem. Soc., Dalton Trans.* **1990**, 1597−1605. (c) Chaudhuri, P.; Winter, M.; Vedova, B. P. C. D.; Bill, E.; Trautwein, A.; Gehring, S.; Fleischhauer, P.; Nuber, B.; Weiss, J. *Inorg. Chem.* **1991**, *30*, 2148−2157. (d) Chaudhuri, P.; Karpenstein, I.; Winter, M.; Butzlaff, C.; Bill, E.; Trautwein, A. X.; Florke, U.; Haupt, H.-J. *J. Chem. Soc., Chem. Commun.* **1992**, 321−22. (e) Chaudhuri, P.; Karpenstein, I.; Winter, M.; Lengen, M.; Butzlaff, C.; Bill, E.; Trautwein, A. X.; Florke, U.; Haupt, H. *Inorg. Chem.* **1993**, *32*, 88−894.

(28) Chaudhuri, P.; Oder, K. *J. Organomet. Chem.* **1989**, *367*, 249−258.

(29) Stevens, R. E.; Gladfelter, W. L. *Inorg. Chem.* **1983**, *22*, 2034−2042.

(30) Brookhart, M.; Grant, B.; Volpe, A. F., Jr. *Organometallics* **1992**, *11*, 3920−3922.

(PF_6) failed. Parenthetically, we note that reactivity differences arising from the divergent steric and/or electronic properties of $L^{i\text{-}Pr_3}$ and L^{Bn_3} have also arisen in ongoing studies of the interactions of $[LCu(CH_3CN)]X$ (X = PF_6 or other anions) with O_2.[31]

Issues raised during mechanistic studies of NO evolution from $L^{i\text{-}Pr_3}Cu(NO_2)$ (see below) raised the question of whether the mixed-valent dimer $[(L^{i\text{-}Pr_3}Cu)_2(\mu\text{-}NO_2)]^{2+}$ could be accessed by treatment of mononuclear $L^{i\text{-}Pr_3}Cu(NO_2)$ with a $L^{i\text{-}Pr_3}Cu^{II}$ fragment that contained labile counterion or solvent coligands. Such a precursor, $L^{i\text{-}Pr_3}Cu(O_3SCF_3)_2$, was prepared by admixture of $L^{i\text{-}Pr_3}$ and $Cu(O_3SCF_3)_2$ in dry THF. Recrystallization from wet solvents or performing the reaction in wet acetone yielded the aquo complex, $[L^{i\text{-}Pr_3}Cu(H_2O)(O_3SCF_3)]O_3SCF_3$, which was characterized by X-ray crystallography. Analogous facile interconversions among $L^{i\text{-}Pr_3}Cu(O_3SCF_3)_2$ and mono- and disolvated forms were supported by conductivity measurements, which indicated that the complex is neutral in CH_2Cl_2 (i.e., both $CF_3SO_3^-$ anions coordinated), a 1:1 electrolyte in acetone, and a 2:1 electrolyte in CH_3CN. Ready displacement of the coordinated $CF_3SO_3^-$ anions in anhydrous $L^{i\text{-}Pr_3}Cu(O_3SCF_3)_2$ in CH_2Cl_2 by the exposed nitrite oxygen atom lone pairs in $L^{i\text{-}Pr_3}Cu(NO_2)$ also was possible, affording mixed valent $[(L^{i\text{-}Pr_3}Cu)_2(\mu\text{-}NO_2)](O_3SCF_3)_2$ in quantitative yield (UV−vis and EPR spectroscopy; see below). Analogous synthetic approaches to multimetal cyanide-bridged assemblies have been reported.[32] A diamagnetic, heterodinuclear analog of the dicopper(I,II) species, $[L^{i\text{-}Pr_3}Cu(\mu\text{-}NO_2)ZnL^{i\text{-}Pr_3}](O_3SCF_3)_2$, was prepared similarly, via admixture of $L^{i\text{-}Pr_3}$, $Zn(O_3SCF_3)_2$, and $L^{i\text{-}Pr_3}Cu(NO_2)$ in CH_2Cl_2 (Scheme 1). As described in detail below, comparison of the properties of the copper(I)−zinc(II) complex with those of the structurally analogous dicopper(I,II) compound proved to be useful for assignment of key spectroscopic features arising from their respective nitrite-bridged cores.

Finally, a monomeric copper(II)−acetate complex, $L^{i\text{-}Pr_3}Cu(O_2CCH_3)_2$, was prepared by mixing $L^{i\text{-}Pr_3}$ and cupric acetate in MeOH. This hygroscopic complex was characterized by spectroscopy, conductivity measurements (neutral in CH_3CN), and X-ray crystallography, allowing its identification as a byproduct of the NO-evolving reaction of $L^{i\text{-}Pr_3}Cu(NO_2)$ with acetic acid (see below).

X-ray Crystallography. The X-ray crystal structures of $[(L^{i\text{-}Pr_3}Cu)_2(\mu\text{-}NO_2)]PF_6$,[21a] $L^{i\text{-}Pr_3}Cu(NO_2)$,[21b] and $L^{i\text{-}Pr_3}Cu(O_2CCH_3)_2$[21b] were reported previously; for reference, drawings are provided in Figures 3 and 4 (see the supporting information associated with the original references for the complete data). New crystallographic data for $[(L^{i\text{-}Pr_3}Cu)_2(\mu\text{-}NO_2)][B(3,5\text{-}(CF_3)_2C_6H_3)_4]_2$, $[L^{i\text{-}Pr_3}Cu(H_2O)(O_3SCF_3)]O_3SCF_3$, and $[L^{i\text{-}Pr_3}Cu(\mu\text{-}NO_2)ZnL^{i\text{-}Pr_3}](O_3SCF_3)_2$ are listed in Tables 1 and 2, with drawings shown in Figures 4−6. Complete listings of positional parameters, temperature factors, and bond distances and angles for these compounds are provided as supporting information.

A. Nitrite Complexes $[(L^{i\text{-}Pr_3}Cu)_2(\mu\text{-}NO_2)]PF_6$, $L^{i\text{-}Pr_3}Cu(NO_2)$, $[(L^{i\text{-}Pr_3}Cu)_2(\mu\text{-}NO_2)][B(3,5\text{-}(CF_3)_2C_6H_3)_4]_2$, and $[L^{i\text{-}Pr_3}Cu(\mu\text{-}NO_2)ZnL^{i\text{-}Pr_3}](O_3SCF_3)_2$. The cores of these molecules are grouped for comparison in Figure 6, with selected bond distances and angles noted. In each complex a pseudotetrahedral Cu^I ion is bonded to the N atom of a nitrite ion. The key differentiating features among the compounds are the presence or absence of an additional nitrite O-bound metal ion and the corresponding nitrite binding mode. As in other triazacyclononane complexes of copper(I),[28] the coordination geometries of the Cu^I ions in all four molecules are best described as C_{3v}-distorted tetrahedral, the principal distortions from idealized tetrahedral local symmetry being (i) intraligand ($L^{i\text{-}Pr_3}$) N−Cu−N bond angles significantly smaller than those between the $L^{i\text{-}Pr_3}$ N atoms and the fourth nitrite donor [average N_L−Cu−N_L = 86.1° vs average N_L−Cu−$N(O)_{nitrite}$ = 127.7°] and (ii) similar Cu−N_L bond distances (average = 2.13 Å) which are typical for Cu^I−N bond lengths in 4-coordinate complexes (∼2.1 Å)[23] but which are significantly longer than the Cu−$O_{nitrite}$ or Cu−$N_{nitrite}$ bonds.

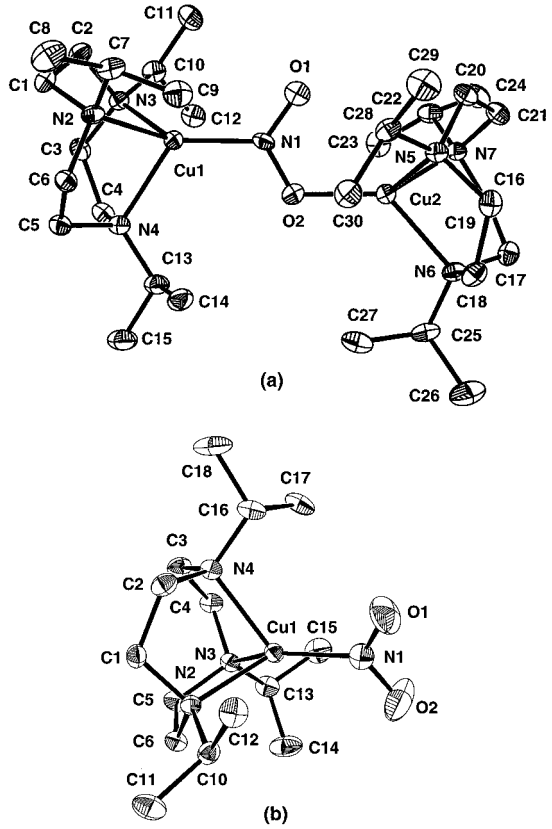

Figure 3. Representations of the X-ray crystal structures of (a) the cation in $[(L^{i\text{-}Pr_3}Cu)_2(\mu\text{-}NO_2)]PF_6$ and (b) $L^{i\text{-}Pr_3}Cu(NO_2)$, showing all nonhydrogen atoms as 50% ellipsoids.

Consideration of the metrical parameters of the mono- and dicopper−nitrite units within each complex reveals distinct features associated with the various nitrite binding modes. In the simplest species, $L^{i\text{-}Pr_3}Cu(NO_2)$, nitrite is bound to a single copper(I) ion solely via its N atom ("nitro" coordination),[33] with a short Cu−$N_{nitrite}$ bond [1.903(4) Å]. Transition metal M−$N_{nitrite}$ bond lengths are usually somewhat longer,[33,34] although examples of short distances have been reported [cf. (TpivPP)-Fe(NO_2), with Fe−$N_{nitrite}$ = 1.849(6) Å].[35] The short distance in the latter species and in $L^{i\text{-}Pr_3}Cu(NO_2)$ presumably reflects an increased M−NO_2 bond order arising from π-back-donation from filled metal orbitals to the lowest energy nitrite π^* orbital (*vide infra*). Significantly longer Cu−$N_{nitrite}$ bonds (≥2.0 Å) have been reported for various salts of the Cu(II) species $Cu(NO_2)_n^{x-}$ (n = 5, x = 3; n = 6, x = 4), although disorders

(31) (a) Mahapatra, S.; Halfen, J. A.; Wilkinson, E. C.; Que, L., Jr.; Tolman, W. B. *J. Am. Chem. Soc.* **1994**, *116*, 9785−9786. (b) Mahapatra, S.; Halfen, J. A.; Wilkinson, E. C.; Pan, G.; Cramer, C. J.; Que, L., Jr.; Tolman, W. B. *J. Am. Chem. Soc.* **1995**, *117*, 8865−8866.

(32) (a) Scott, M. J.; Holm, R. H. *J. Am. Chem. Soc.* **1994**, *116*, 11357−11367. (b) Scott, M. J.; Lee, S. C.; Holm, R. H. *Inorg. Chem.* **1994**, *33*, 4651−4662.

(33) Hitchman, M. A.; Rowbottom, G. L. *Coord. Chem. Rev.* **1982**, *42*, 55−132.

(34) Allen, F. H.; Kennard, O.; Watson, D. G.; Brammer, L.; Orpen, A. G.; Taylor, R. *J. Chem. Soc., Perkin Trans.* **1987**, S1−S19.

(35) Nasri, H.; Wang, Y.; Huynh, B. H.; Scheidt, W. R. *J. Am. Chem. Soc.* **1991**, *113*, 719−721.

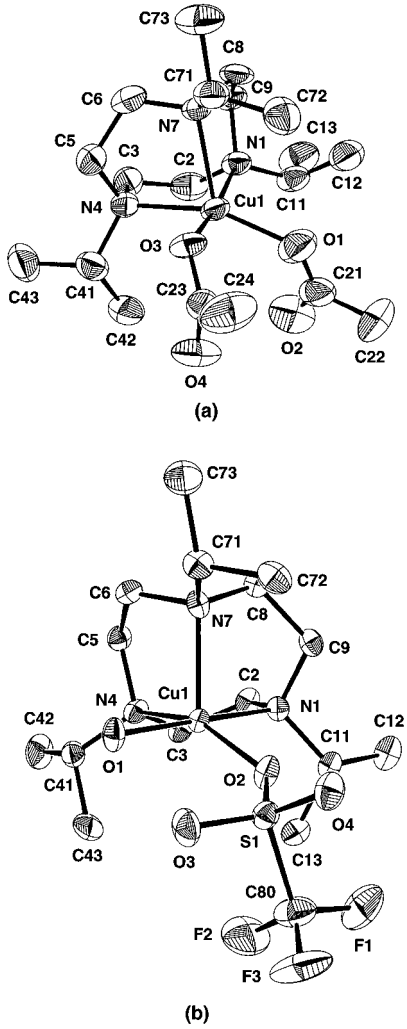

Figure 4. Representations of the X-ray crystal structures of (a) $L^{i\text{-}Pr_3}Cu(O_2CCH_3)_2$ and (b) the cation in $[L^{i\text{-}Pr_3}Cu(H_2O)(O_3SCF_3)]O_3SCF_3$, showing all nonhydrogen atoms as 50% ellipsoids.

involving possible static and/or dynamic Jahn-Teller distortions complicate comparisons to crystallographic data obtained for many of these compounds.[36] Finally, as is typical for transition metal nitro complexes,[33] in $L^{i\text{-}Pr_3}Cu(NO_2)$, the nitrite O−N−O angle [116.0(2)°] and N−O distances [1.253(5) and 1.238(5) Å] differ only slightly from those of the free nitrite ion [114.9(5)° and 1.240(3) Å, respectively],[37] the approximate equivalence of the distances being consistent with the expected lack of bond alternation.

Increased N−O bond alternation is evident in the structure of $[(L^{i\text{-}Pr_3}Cu)_2(\mu\text{-}NO_2)]PF_6$, in which a nitrite ion bridges two copper(I) ions via its N atom and a *syn* lone pair on one O atom to afford a planar $Cu^I-(\mu\text{-}NO_2)-Cu^I$ array [N−O = 1.235(3) and 1.279(3) Å; Δ(N−O) = 0.044 Å vs 0.015 for $L^{i\text{-}Pr_3}Cu(NO_2)$]. Weak or nonexistent bonding between O1 and the metal ions is evident from the approximately C_{3v}-symmetric copper(I) geometries and the long O1−Cu distances [2.786(2) and 2.820(2) Å to Cu1 and Cu2, respectively]. The μ-(η^1-*N*:η^1-*O*)-nitrite coordination mode observed for the complex is unusual in transition metal chemistry;[38] related μ-(η^1-*N*:η^1-*O*)-nitrite bridges in which the *anti* (instead of the *syn*) lone pair on the O atom is coordinated occur in the presence of additional bridging ligands.[39] In the only other example of a complex containing a $Cu^I-O_{nitrite}$ bond, $[(PPh_3)_2Cu(\eta^2\text{-}O,O\text{-}NO_2)]$,[40] the Cu−O distance [2.191(4) Å] is significantly longer than in $[(L^{i\text{-}Pr_3}Cu)_2(\mu\text{-}NO_2)]PF_6$ [1.968(2) Å], perhaps reflecting the contrasting η^2 vs η^1 binding modes and/or divergent interligand steric influences. The $Cu-N_{nitrite}$ bond length in the dinuclear complex, 1.899(2) Å, is identical to that in $L^{i\text{-}Pr_3}Cu(NO_2)$ within experimental error. Thus, the binding of an additional copper(I) ion to the O atom of the nitrite ligand appears to have a negligible effect on the $Cu-N_{nitrite}$ bonding, despite its influence on the degree of NO_2^- N−O bond alternation.

Table 1. Selected Bond Lengths (Å) and Angles (deg) for Complexes Characterized by X-ray Crystallography[a]

$[L^{i\text{-}Pr_3}Cu(H_2O)(O_3SCF_3)]O_3SCF_3$			
Cu(1)−O(1)	2.014(5)	Cu(1)−O(2)	2.052(4)
Cu(1)−N(1)	2.046(5)	Cu(1)−N(4)	2.070(5)
Cu(1)−N(7)	2.180(5)	S(1)−O(2)	1.472(4)
S(1)−O(3)	1.438(5)	S(1)−O(4)	1.431(4)
O(1)−Cu(1)−O(2)	86.9(2)	O(1)−Cu(1)−N(1)	178.6(2)
O(1)−Cu(1)−N(4)	94.9(2)	O(1)−Cu(1)−N(7)	93.9(2)
O(2)−Cu(1)−N(1)	91.8(2)	O(2)−Cu(1)−N(4)	157.7(2)
O(2)−Cu(1)−N(7)	113.2(2)	N(1)−Cu(1)−N(4)	86.3(2)
N(1)−Cu(1)−N(7)	86.8(2)	N(4)−Cu(1)−N(7)	88.9(2)
O(2)−S(1)−O(3)	114.0(3)	O(2)−S(1)−O(4)	112.8(3)
O(3)−S(1)−O(4)	117.6(3)	Cu(1)−O(2)−S(1)	140.5(3)
$[(L^{i\text{-}Pr_3}Cu)_2(\mu\text{-}NO_2)][B(3,5\text{-}(CF_3)_2C_6H_3)_4]_2$			
Cu(1′)−O(1)	2.047(9)	Cu(1′)−O(2)	2.13(1)
Cu(1)−N(1)	1.780(8)	Cu(1)−N(2)	2.069(5)
Cu(1)−N(3)	2.104(6)	Cu(1)−N(4)	2.051(6)
O(1)−N(1)	1.26(1)	O(2)−N(1)	1.30(1)
O(1)−Cu(1′)−O(2)	60.2(3)	O(1)−Cu(1′)−N(2′)	153.5(3)
O(1)−Cu(1′)−N(3′)	107.9(3)	O(1)−Cu(1′)−N(4′)	113.1(3)
O(2)−Cu(1′)−N(2′)	93.5(3)	O(2)−Cu(1′)−N(3′)	122.3(3)
O(2)−Cu(1′)−N(4′)	148.7(3)	N(1)−Cu(1)−N(2)	126.4(4)
N(1)−Cu(1)−N(3)	120.8(4)	N(1)−Cu(1)−N(4)	132.0(4)
N(2)−Cu(1)−N(3)	88.8(2)	N(2)−Cu(1)−N(4)	86.9(2)
N(3)−Cu(1)−N(4)	89.1(2)	Cu(1′)−O(1)−N(1)	97.4(7)
Cu(1′)−O(2)−N(1)	92.3(7)	Cu(1)−N(1)−O(2)	125.4(9)
Cu(1)−N(1)−O(1)	124.3(9)	O(1)−N(1)−O(2)	110.1(7)
$[L^{i\text{-}Pr_3}Cu(\mu\text{-}NO_2)ZnL^{i\text{-}Pr_3}](O_3SCF_3)_2$			
Zn(1)−N(5)	1.998(3)	Zn(1)−O(1)	2.031(3)
Zn(1)−N(6)	2.039(3)	Zn(1)−O(2)	2.044(3)
Zn(1)−N(7)	2.161(3)	Cu(1)−N(1)	1.848(3)
Cu(1)−N(2)	2.095(3)	Cu(1)−N(3)	2.050(3)
Cu(1)−N(4)	2.143(3)	N(1)−O(1)	1.269(4)
N(1)−O(2)	1.274(4)	N(5)−Zn(1)−O(1)	99.43(11)
N(5)−Zn(1)−N(6)	88.34(12)	O(1)−Zn(1)−N(6)	156.05(11)
N(5)−Zn(1)−O(2)	161.71(11)	O(1)−Zn(1)−O(2)	62.28(10)
N(6)−Zn(1)−O(2)	108.30(11)	N(5)−Zn(1)−N(7)	88.64(12)
O(1)−Zn(1)−N(7)	113.84(11)	N(6)−Zn(1)−N(7)	88.80(12)
O(2)−Zn(1)−N(7)	98.98(11)	N(5)−Zn(1)−N(1)	130.49(11)
N(6)−Zn(1)−N(1)	136.39(11)	N(7)−Zn(1)−N(1)	108.27(11)
N(1)−Cu(1)−N(3)	125.03(14)	N(1)−Cu(1)−N(2)	135.57(14)
N(3)−Cu(1)−N(2)	87.9(2)	N(1)−Cu(1)−N(4)	120.20(12)
N(3)−Cu(1)−N(4)	87.78(12)	N(2)−Cu(1)−N(4)	86.01(12)
O(1)−N(1)−O(2)	111.9(3)	O(1)−N(1)−Cu(1)	122.5(2)
O(2)−N(1)−Cu(1)	125.3(2)	N(1)−O(1)−Zn(1)	93.2(2)
N(1)−O(2)−Zn(1)	92.5(2)		

[a] Estimated standard deviations are given in parentheses.

(36) (a) Ozarowski, A.; Allmann, R.; Pour-Ibrahim, A.; Reinen, R. Z. *Anorg. Allg. Chem.* **1991**, *592*, 187−201. (b) Klein, S.; Reinen, D. *J. Solid State Chem.* **1980**, *32*, 311−319. (c) Cullen, D. L.; Lingafelter, E. C. *Inorg. Chem.* **1971**, *10*, 1264−1268. (d) Takagi, S.; Joesten, M. D.; Lenhert, P. G. *J. Am. Chem. Soc.* **1975**, *97*, 444−445. (e) Takagi, S.; Joesten, M. D.; Lenhert, P. G. *Acta Crystallogr.* **1975**, *B31*, 596−598.

(37) Kay, M. I.; Frazer, B. C. *Acta Crystallogr.* **1961**, *B24*, 56.

(38) (a) Finney, A. J.; Hitchman, M. A.; Raston, C. L.; Rowbottom, G. L.; White, A. H. *Aust. J. Chem.* **1981**, *34*, 2163. (b) Drew, M. G. B.; Goodgame, D. M. L.; Hitchman, M. A.; Rogers, D. *J. Chem. Soc., Chem. Commun.* **1965**, 477. (c) Strouse, C. E.; Swanson, B. I. *J. Chem. Soc., Chem. Commun.* **1971**, 55.

(39) (a) Johnson, B. F.; Sieker, A.; Blake, A. J.; Winpenny, R. E. P. *J. Chem. Soc., Chem. Commun.* **1993**, 1345−1346. (b) Thewalt, U.; Marsh, R. E. *Inorg. Chem.* **1970**, *9*, 1604−1610. (c) Goodgame, D. M. L.; Hitchman, M. A.; Marsham, D. F.; Phavanantha, P.; Rogers, D. *J. Chem. Soc., Chem. Commun.* **1969**, 1383−1384.

(40) Halfen, J. A.; Tolman, W. B. *Acta Crystallogr.* **1995**, *C51*, 215−217.

Table 2. Summary of X-ray Crystallographic Data

complex	$[L^{i\text{-}Pr_3}Cu(H_2O)(O_3SCF_3)]O_3SCF_3$	$[(L^{i\text{-}Pr_3}Cu)_2(\mu\text{-}NO_2)][B(3,5\text{-}(CF_3)_2C_6H_3)_4]_2$	$[L^{i\text{-}Pr_3}Cu(\mu\text{-}NO_2)ZnL^{i\text{-}Pr_3}](O_3SCF_3)_2$
emp form	$C_{17}H_{35}CuF_6N_3O_7S_2$	$C_{94}H_{90}B_2Cu_2F_{48}N_7O_2$	$C_{32}H_{66}CuF_6N_7O_8S_2Zn$
fw	635.14	2410.43	983.95
cryst syst	monoclinic	triclinic	monoclinic
space group	$P2_1/c$	$P\bar{1}$	$P2_1/c$
a (Å)	8.59(1)	13.439(8)	10.8752(1)
b (Å)	26.04(1)	13.777(5)	15.6121(3)
c (Å)	12.838(4)	14.471(8)	25.8020(5)
α (deg)		108.22(4)	
β (deg)	108.26(6)	92.08(5)	90.094(1)
γ (deg)		90.08(4)	
V (Å^3)	2727(6)	2543(4)	4380.78(13)
Z	4	1	4
density (calcd)	1.547 g/cm^3	1.574 g/cm^3	1.492 g/cm^3
temp (K)	173(2)	177(2)	173(2)
crystal size (mm)	0.57 × 0.47 × 0.31	0.60 × 0.35 × 0.30	0.50 × 0.16 × 0.12
diffractometer	Enraf-Nonius CAD-4	Enraf-Nonius CAD-4	Siemens SMART
radiation	Mo Kα (λ = 0.71073 Å)	Mo Kα (λ = 0.71069 Å)	Mo Kα (λ = 0.71073 Å)
absn coeff	10.27 cm^{-1}	5.53 cm^{-1}	1.207 mm^{-1}
2θ max (deg)	56.0	52.0	48.26
no. of reflns colld	8540	10436	17862
no. of ind reflns	6704	9956	6851
no. of obsd reflns	4111 [$I > 2\sigma(I)$]	6113 [$I > 2\sigma(I)$]	6849
params	326	715	622
$R1$[a] [$I > 2\sigma(I)$]	0.067	0.074	0.0472
Rw[a]	0.064	0.070	
w$R2$[b] [$I > 2\sigma(I)$]			0.1082
goodness-of-fit	1.61	1.80	1.122
largest diff peak and hole (e Å^{-3})	1.10; −1.27	0.65; −0.54	0.438; −0.332

[a] $R1 = \sum||F_o| - |F_c||/\sum|F_o|$; $Rw = [(\sum w(|F_o| - |F_c|)^2/\sum wF_o^\infty)]^{1/2}$, where $w = 4F_o^2/\sigma^2(F_o^2)$; $\sigma^2(F_o^2) = [S^2(C + R^2B) + (pF_o^2)^2]/Lp^2$; S = scan rate, C = total integrated peak count, R = ratio of scan time to background counting time, B = total background count, Lp = Lorentz−polarization factor, and p = p factor. [b] $wR2 = [\sum[w(F_o^2 - F_c^2)^2]/\sum[w(F_o^2)^2]]^{1/2}$, where $w = q/\sigma^2(F_o^2) + (aP)^2 + bP$.

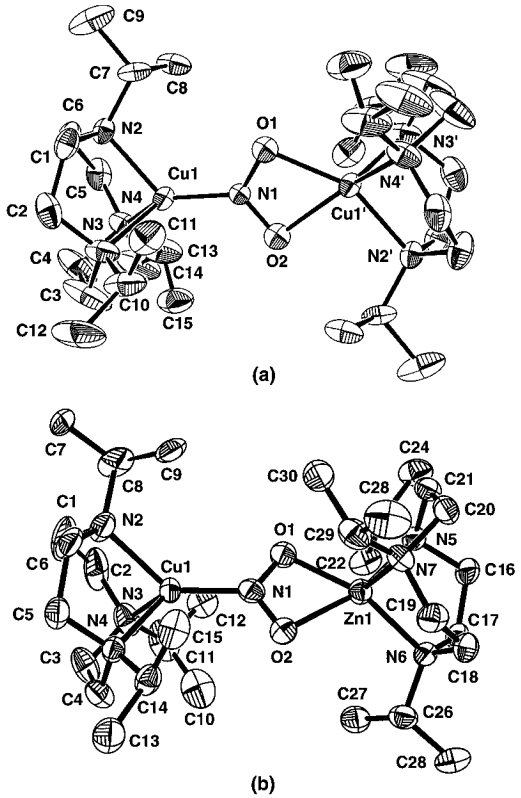

Figure 5. Representations of the X-ray crystal structures of the cations of (a) $[(L^{i\text{-}Pr_3}Cu)_2(\mu\text{-}NO_2)][B(3,5\text{-}(CF_3)_2C_6H_3)_4]_2$ and (b) $[L^{i\text{-}Pr_3}Cu(\mu\text{-}NO_2)ZnL^{i\text{-}Pr_3}](O_3SCF_3)_2$, showing all nonhydrogen atoms as 50% ellipsoids.

A shift in the binding mode of the bridging nitrite induced by one-electron oxidation of the dicopper(I,I) complex is evident from the X-ray crystal structure of mixed valent $[(L^{i\text{-}Pr_3}Cu)_2(\mu\text{-}NO_2)][B(3,5\text{-}(CF_3)_2C_6H_3)_4]_2$ (Figures 5 and 6). The complex crystallizes in the centrosymmetric space group $P\bar{1}$ with a crystallographic inversion center within the cation, thus indicating "end-for-end" disorder. Location of peaks in difference Fourier maps corresponding to the two possible orientations of the bridging nitrite ligand allowed successful modeling of the disorder (see the Experimental Section). The novel μ-(η^1-*N*:η^2-*O*,*O*)-nitrite bonding geometry in the complex is characterized by a remarkably short $Cu-N_{nitrite}$ bond distance [1.780(8) Å], only slightly asymmetric *O*,*O*-chelation to the other copper center [Cu1′−O1 = 2.047(9) Å; Cu1′−O2 = 2.13(1) Å], and a planar $Cu_2(NO_2)$ core with a Cu···Cu separation of 4.31 Å. This nitrite binding mode is, to our knowledge, unprecedented in transition metal chemistry; the few known examples of such a topology involve Pb^{II} or Cd^{II} ions.[41]

A description of crystalline $[(L^{i\text{-}Pr_3}Cu)_2(\mu\text{-}NO_2)]^{2+}$ as completely valence localized (class I)[42] appears appropriate on the basis of the divergent coordination geometries of the copper ions that are characteristic for their respective 1+ and 2+ oxidation levels. Thus, we assign a 1+ oxidation state to Cu1 because it is roughly tetrahedral, with L−Cu−L bond angles similar to those observed for $L^{i\text{-}Pr_3}Cu(NO_2)$ and $[(L^{i\text{-}Pr_3}Cu)_2(\mu\text{-}NO_2)]PF_6$. A distorted 5-coordinate square pyramidal geometry for Cu1′ is consistent with its Cu^{II} designation. This preference for coordination of the nitrite N atom to Cu^{I} and the O atoms to Cu^{II} is in accord with simple hard−soft acid−base considerations.

Our assessment of the valence localization in the dicopper(I,II) complex is corroborated by the congruence between its

(41) (a) Shvelashvili, A. E.; Porai-koshits, M. A. *Koord. Khim.* **1975**, *1*, 467. (b) Nardelli, M.; Pelizzi, G. *Inorg. Chim. Acta* **1980**, *38*, 15. (c) Takagi, S.; Joesten, M.; Lenhert, P. G. *Acta Crystallogr.* **1976**, *B32*, 326, 1278. (d) Cullen, D. L.; Lingafelter, E. C. *Inorg. Chem.* **1971**, *10*, 1264−1268.

(42) Robin, M. B.; Day, P. *Adv. Inorg. Chem. Radiochem.* **1967**, *10*, 247−422.

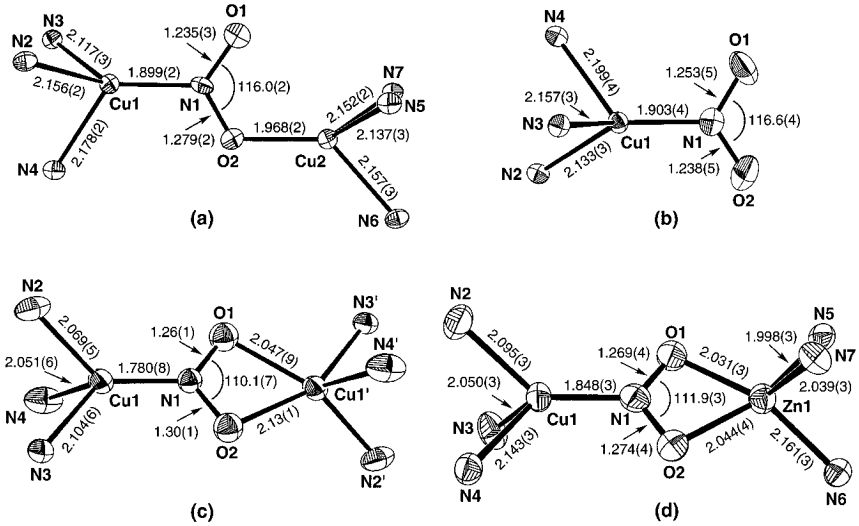

Figure 6. Drawings with selected bond distances (Å) and angles (deg) noted of the cores of (a) $[(L^{i\text{-}Pr_3}Cu)_2(\mu\text{-}NO_2)]PF_6$, (b) $L^{i\text{-}Pr_3}Cu(NO_2)$, (c) $[(L^{i\text{-}Pr_3}Cu)_2(\mu\text{-}NO_2)][B(3,5\text{-}(CF_3)_2C_6H_3)_4]_2$, and (d) $[L^{i\text{-}Pr_3}Cu(\mu\text{-}NO_2)ZnL^{i\text{-}Pr_3}](O_3SCF_3)_2$.

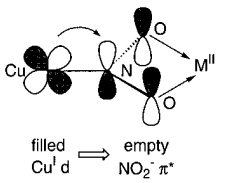

Cu-N (Å)	M^{II}	λ_{max} MLCT (nm)
1.903(4)	--	<350
1.848(3)	Zn	406
1.780(8)	Cu	444

Figure 7. Qualitative view of the back-bonding interaction between Cu^I and nitrite in $L^{i\text{-}Pr_3}Cu(NO_2)$ and the mixed valent Cu^ICu^{II} and Cu^I-Zn^{II} complexes, with related structural and spectroscopic features listed (see Discussion).

structure and that of $[L^{i\text{-}Pr_3}Cu(\mu\text{-}NO_2)ZnL^{i\text{-}Pr_3}](O_3SCF_3)_2$ (Figures 5 and 6), which is constrained to a Cu^IZn^{II} formulation by the inaccessibility of oxidation states other than 2+ for zinc. The high degree of similarity between the two structures is striking, the only significant difference between them being the Cu−$N_{nitrite}$ bond length [1.780(8) vs 1.848(3) Å for the Cu^ICu^{II} and Cu^IZn^{II} complexes, respectively]. Consideration of these different Cu−$N_{nitrite}$ bond distances, in conjunction with the corresponding 1.903(4) Å bond length in $L^{i\text{-}Pr_3}Cu(NO_2)$, reveals a clear trend that reflects the nature of the *O,O*-nitrite bonding. The shortest distance is found for the case where Cu^{II} is coordinated to the nitrite O atoms and the longest occurs for the monomer, which has no *O*-bound metal ions, with the distance for the Cu^IZn^{II} complex falling between these extremes. Single *O*-nitrite coordination as in the dicopper(I,I) complex apparently does not perturb the system sufficiently to affect the Cu−$N_{nitrite}$ bond distance. The correlation between *O,O*-nitrite coordination and Cu^I−$N_{nitrite}$ bond length can be rationalized by invoking an effect of *O,O*-binding on the π-back-bonding between the copper(I) ion and the N-bound nitrite ligand (Figure 7). As the strength of *O,O*-nitrite coordination by the divalent metal ion increases (Cu^{II} > Zn^{II} > none), the energy of the nitrite π^* orbital of appropriate symmetry to interact with a filled copper(I) orbital would be expected to decrease due to the electron-withdrawing influence of the *O,O*-bound metal, thus resulting in stronger $Cu^I \rightarrow N_{nitrite}$ back-bonding and a correspondingly shorter Cu^I−$N_{nitrite}$ bond length. Although direct experimental evidence for the stronger bonding to $L^{i\text{-}Pr_3}Cu(NO_2)$ by the $L^{i\text{-}Pr_3}Cu^{II}$ fragment compared to $L^{i\text{-}Pr_3}Zn^{II}$ is lacking, such a bond strength order is consistent with the Irving−Williams series[43] and with the known greater stability of bidentate coordination of nitrate to N_3M^{II} moieties when $M^{II} = Cu^{II}$ vs Zn^{II}.[44] As described below, this qualitative bonding description (Figure 7) also accounts for observed differences in spectroscopic properties among the various copper(I) nitrite complexes.

B. $[L^{i\text{-}Pr_3}Cu(H_2O)(O_3SCF_3)]O_3SCF_3$. The structure of this compound (Figure 4b) reveals a typical 5-coordinate distorted square pyramidal copper(II) ion with one $L^{i\text{-}Pr_3}$ N atom (N7) occupying the pseudoaxial position at a Cu−N distance [2.180(5) Å] significantly longer than the other two (average 2.06 Å). A water molecule and a monodentate triflate ion complete the coordination sphere of this additional member of a growing class of crystallographically characterized copper(II) triflates supported by tridentate N-donor ligands.[18b,32] The aquo ligand appears to be hydrogen-bonded to both the coordinated and uncoordinated triflate groups, as indicated by the O1···O3 and O1···O7 distances of 2.73 and 2.72 Å, respectively (aquo H atoms not found). Similar patterns of hydrogen bonding to triflate ions in aquo complexes have been reported.[45] Also similar to other transition metal triflate complexes,[47] the S−O distances reflect O atom coordination (S1−O2 longer than S1−O3 or S1−O4 by >0.03 Å).

NMR and EPR Spectroscopy. ^1H and ^{13}C NMR spectroscopy were found to be particularly useful for elucidation of the structures of the diamagnetic copper(I) complexes in solution. We assign C_{3v}-distorted pseudotetrahedral geometries to $[LCu(CH_3CN)]PF_6$ (L = $L^{i\text{-}Pr_3}$ or L^{Bn_3}) and $[L^{i\text{-}Pr_3}Cu(PPh_3)]PF_6$ on the basis of the number of resonances in their $^{13}C\{^1H\}$ NMR spectra, the pattern of ligand substituent peaks in their ^1H NMR spectra (cf. one doublet/heptet set for the isopropyl substituents for L = $L^{i\text{-}Pr_3}$), and diagnostic features in NMR and IR spectra consistent with coordinated CH_3CN or PPh_3. In addition, comparison of the ^1H NMR data for the free ligands to those for the complexes reveals differences in the methylene backbone region that are diagnostic for metal ion binding. For example, a single peak at 2.5 ppm for $L^{i\text{-}Pr_3}$ is split into multiplets centered at 2.80 and 2.55 ppm upon binding to copper(I) to yield $[L^{i\text{-}Pr_3}Cu(CH_3CN)]PF_6$. NMR spectra similar to those observed for the copper(I) starting materials were recorded for the nitrite

(43) Sigel, H.; McCormick, D. B. *Acc. Chem. Res.* **1970**, *3*, 201−208.
(44) (a) Han, R.; Parkin, G. *J. Am. Chem. Soc.* **1991**, *113*, 9707−9708. (b) Looney, A.; Parkin, G. *Inorg. Chem.* **1994**, *33*, 1234−1237.
(45) For a recent example, see: Stang, P. J.; Cao, D. H.; Poulter, G. T.; Arif, A. M. *Organometallics* **1995**, *14*, 1110−1114 and references cited therein.
(46) Lawrance, G. A. *Chem. Rev.* **1986**, *86*, 17−33.

Table 3. Summary of Selected Spectroscopic Data

complex	EPR[a]	UV−vis[b]	FTIR[c]	resonance Raman[c]
$[(L^{i\text{-}Pr_3}Cu)_2(\mu\text{-}NO_2)]PF_6$		338 (3000), 380 (2200)	1352 (1333), 1185 (1168)	
$[(L^{Bn_3}Cu)_2(\mu\text{-}NO_2)]PF_6$		336 (3700)	1347 (1331), 1202 (1174)	
$[(L^{i\text{-}Pr_3}Cu)_2(\mu\text{-}NO_2)](PF_6)_2$	$g_\perp = 2.07$, $g_\parallel = 2.24$, $A_\parallel = 136 \times 10^{-4}$	314 (3900), 356 (sh, 3000), 444 (2500), 668 (320)	1235 (1214)	1238 (1218), 876 (874)
$[L^{i\text{-}Pr_3}Cu(\mu\text{-}NO_2)ZnL^{i\text{-}Pr_3}](CF_3SO_3)_2$		406 (2200), 358 (1900)	*d*	1238 (1214), 872 (868)
$L^{i\text{-}Pr_3}Cu(NO_2)$		308 (3800)	1306,[e] 1268 (1247)	
$L^{i\text{-}Pr_3}Cu(O_2CCH_3)_2$	$g_\perp = 2.06$, $g_\parallel = 2.30$, $A_\parallel = 154 \times 10^{-4}$	298 (4900), 684 (110)		
$L^{i\text{-}Pr_3}Cu(O_3SCF_3)_2$	$g_\perp = 2.09$, $g_\parallel = 2.28$, $A_\parallel = 160 \times 10^{-4}$	300 (3600), 718 (100)		

[a] $A_\parallel$ values quoted in cm^{-1}; measured at 77 K as 1:1 CH_2Cl_2/toluene glasses. [b] λ_{max}, nm (ϵ/complex, M^{-1} cm^{-1}); measured at room temperature as solutions in CH_2Cl_2. [c] ^{15}N-sensitive vibrations quoted in cm^{-1}; measured at room temperature as KBr pellets. [d] ^{15}N-sensitive NO_2^- vibrations obscured by counterion stretches. [e] The corresponding $^{15}NO_2^-$ stretch was obscured by other vibrations.

complexes $L^{i\text{-}Pr_3}Cu(NO_2)$, $[(LCu)_2(\mu\text{-}NO_2)]PF_6$ (L = $L^{i\text{-}Pr_3}$ or L^{Bn_3}), and $[L^{i\text{-}Pr_3}Cu(\mu\text{-}NO_2)ZnL^{i\text{-}Pr_3}](O_3SCF_3)_2$. Despite the asymmetry inherent to the solid state structure of $[(L^{i\text{-}Pr_3}Cu)_2(\mu\text{-}NO_2)]PF_6$, only one set of ligand resonances appeared in its NMR spectrum, suggesting either coincidental overlap of peaks associated with the $N_{nitrite}$- and $O_{nitrite}$-bound copper units or, more likely, rapid fluxionality involving interchange of $L^{i\text{-}Pr_3}$-Cu environments. Although such an interchange may involve mononuclear intermediates, none were observed. In contrast, the ^1H and ^{13}C NMR spectra of $[L^{i\text{-}Pr_3}Cu(\mu\text{-}NO_2)ZnL^{i\text{-}Pr_3}](O_3SCF_3)_2$ in CD_2Cl_2 contained distinct and sharp $L^{i\text{-}Pr_3}$ resonances for the zinc(II) and copper(I) sites, consistent with a lack of exchange of $L^{i\text{-}Pr_3}$ between the Cu^I and Zn^{II} ions.

The mixed valent complex $[(L^{i\text{-}Pr_3}Cu)_2(\mu\text{-}NO_2)](PF_6)_2$ exhibited an axial signal in its 77 K X-band EPR spectrum with parameters typical for a square pyramidal Cu^{II} site with mixed N,O coordination (Table 3).[47] Double integration confirmed that the signal arose from one unpaired electron per complex. The nature of this signal, which showed no evidence for additional hyperfine coupling to a second copper nucleus, is consistent with localization of unpaired spin density on the 5-coordinate copper ion as suggested by the X-ray crystallographic evidence cited above. EPR spectra typical for 5-coordinate Cu^{II} ions in square pyramidal geometries were also recorded for solutions of the mononuclear compounds $L^{i\text{-}Pr_3}Cu(O_3SCF_3)_2$ and $L^{i\text{-}Pr_3}Cu(O_2CCH_3)_2$ in 1:1 CH_2Cl_2/toluene (Table 3).

Electronic Absorption Spectroscopy. In contrast to the colorless $[LCu(CH_3CN)]X$ starting materials and $[L^{i\text{-}Pr_3}Cu(PPh_3)]PF_6$, the copper(I) nitrite adducts are yellow to yellow-orange due to intense absorptions between 308 and 338 nm (ϵ/complex 3000−3800 M^{-1} cm^{-1}) (Table 3). We suggest that these features are $Cu^I \rightarrow NO_2^-$ metal-to-ligand charge transfer (MLCT) transitions, although such assignments remain tentative in the absence of more conclusive evidence such as that which would be provided by resonance Raman spectroscopic experiments (planned). One-electron oxidation of yellow-orange $[(L^{i\text{-}Pr_3}Cu)_2(\mu\text{-}NO_2)]PF_6$ caused a color change to deep red due to a much lower energy absorption in the mixed valent dicopper(I,II) product [Figure 8 and Table 3; $\lambda_{max} = 444$ nm (ϵ/complex 2500 M^{-1} cm^{-1})]. An additional much weaker absorption feature at 668 nm (ϵ/complex 320 M^{-1} cm^{-1}) attributable to a ligand field (dd) transition corroborates the presence of a copper(II) ion in this compound. Resonance Raman spectra of solid $[(L^{i\text{-}Pr_3}Cu)_2(\mu\text{-}NO_2)](PF_6)_2$ (KBr pellet) obtained using 458 nm excitation contained intense features that shifted upon $^{15}NO_2^-$ substitution (see below), clearly indicating that the 444 nm absorption band arises from a charge transfer transition involving

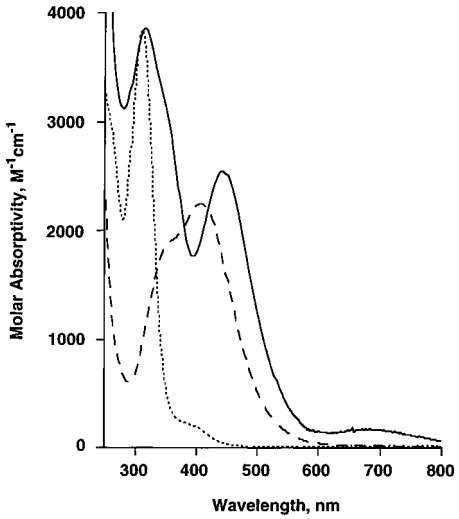

Figure 8. UV−vis spectra of CH_2Cl_2 solutions $L^{i\text{-}Pr_3}Cu(NO_2)$ (···), $[(L^{i\text{-}Pr_3}Cu)_2(\mu\text{-}NO_2)](O_3SCF_3)_2$ (—), and $[L^{i\text{-}Pr_3}Cu(\mu\text{-}NO_2)ZnL^{i\text{-}Pr_3}](O_3SCF_3)_2$ (- - -).

the nitrite ligand. To investigate whether this transition should be designated as a $Cu^I \rightarrow NO_2^-$ MLCT or a $NO_2^- \rightarrow Cu^{II}$ ligand-to-metal charge transfer (LMCT), we prepared and characterized the copper(I)−zinc(II) analog, for which the latter type of transition would be impossible because both metal ions have filled d shells. Like the Cu^ICu^{II} compound, the Cu^IZn^{II} complex is deep red, exhibits an intense electronic absorption at 406 nm (ϵ/complex 2200 M^{-1} cm^{-1}) in CH_2Cl_2 (Figure 8), and gives rise to $^{15}NO_2^-$ isotope sensitive bands in its resonance Raman spectrum upon 458 nm excitation (see below). As expected, the low-energy ligand field band observed for the dicopper(I,II) compound ($\lambda_{max} = 668$ nm) is absent in the spectrum of the heterodinuclear analog. Taken together, these observations allow definitive attribution of the 406 nm band in the copper−zinc salt as a $Cu^I \rightarrow NO_2^-$ MLCT transition and provide convincing, albeit indirect, support for a similar assignment to the 444 nm absorption for the dicopper(I,II) complex.

Agreement between electronic absorption spectroscopic and X-ray structural features lends support for the bonding model cited above for the copper(I) nitrite unit. As depicted in Figure 7, the $Cu^I-N_{nitrite}$ bond length is inversely correlated with MLCT energies in the series (ordered according to the bond distance) $L^{i\text{-}Pr_3}Cu(NO_2) \approx [(L^{i\text{-}Pr_3}Cu)_2(\mu\text{-}NO_2)]PF_6 > [L^{i\text{-}Pr_3}Cu(\mu\text{-}NO_2)ZnL^{i\text{-}Pr_3}](O_3SCF_3)_2 > [(L^{i\text{-}Pr_3}Cu)_2(\mu\text{-}NO_2)](PF_6)_2$. This correlation may be explained by arguing that, as the divalent metal *O*,*O*-nitrite coordination strengthens in the series, more efficient electron withdrawal by the divalent metal ion causes the nitrite π^* orbital to decrease in energy, resulting in a stronger $Cu^I \rightarrow$

(47) Peisach, J.; Blumberg, W. E. *Arch. Biochem. Biophys.* **1974**, *165*, 691−708.

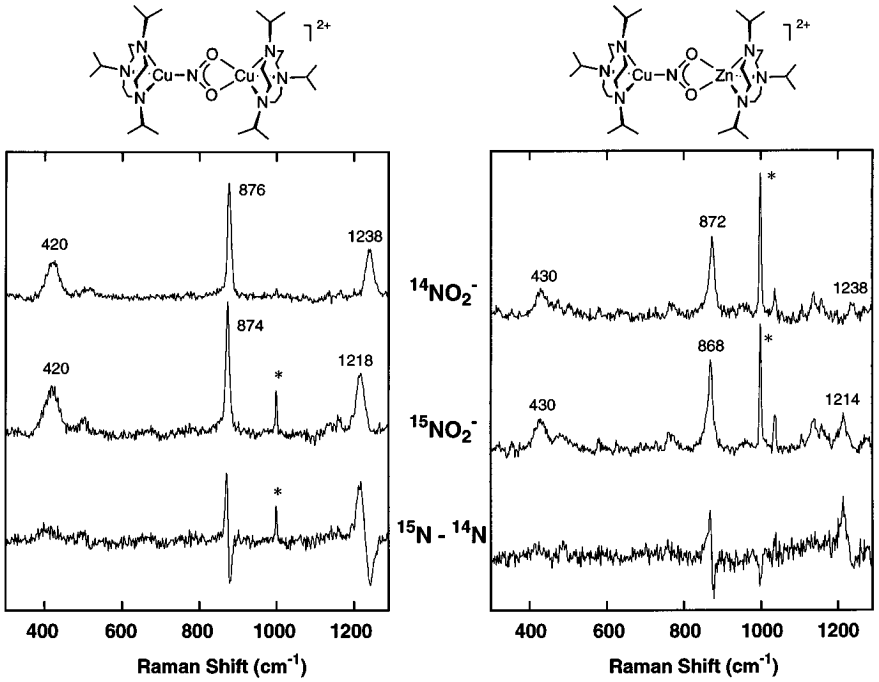

Figure 9. Resonance Raman spectra obtained using 457.9 nm excitation for the $^{14}NO_2^-$ and $^{15}NO_2^-$ isotopomers of the mixed valent dicopper(I,II) and copper(I)−zinc(II) complexes, with difference spectra displayed at the bottom of each set (* denotes the sulfate standard peak).

NO_2^- back-bonding interaction, a shorter $Cu-N_{nitrite}$ bond, and a lower energy (longer wavelength) $Cu^I \rightarrow NO_2^-$ MLCT transition.

Infrared and Resonance Raman Spectroscopy. Pairs of infrared vibrations sensitive to $^{15}NO_2^-$ substitution between 1150 and 1400 cm^{-1} were identified for $L^{i\text{-}Pr_3}Cu(NO_2)$ and $[(LCu)_2(\mu\text{-}NO_2)]PF_6$ ($L = L^{i\text{-}Pr_3}$ and L^{Bn_3}) (Table 3). We tentatively assign the 1306 and 1268 cm^{-1} ^{15}N-sensitive bands in $L^{i\text{-}Pr_3}Cu(NO_2)$ to nitrite asymmetric (ν_{as}) and symmetric (ν_s) stretches, respectively, on the basis of the similarity of their frequencies and/or isotope shifts to features identified in other transition metal η^1-NO_2^- (nitro) complexes such as $[Cu(NO_2)_6]^{4-}$ (∼1330 and ∼1280 cm^{-1}).[33,48] The difference in energy between ν_{as} and ν_s for the dicopper(I,I) complexes is notably greater than for $L^{i\text{-}Pr_3}Cu(NO_2)$, which is consistent with greater N−O bond alternation in the former compounds (see ref 33 for a discussion of the correlation between N−O bond distance differences and the ν_{as}/ν_s vibrational frequency separation in metal nitrite compounds). More definitive assignments for all of the copper(I) compounds await a full analysis incorporating results from resonance Raman spectroscopy using suitable excitation wavelengths in the UV region. In any case, the similarity of the IR data for the dicopper(I,I) complexes capped by $L^{i\text{-}Pr_3}$ and L^{Bn_3} represents important evidence for the postulate of congruent structures for the two molecules.

For the mixed valent dicopper(I,II) and copper(I)−zinc(II) complexes, 458 nm irradiation into their absorption bands (λ_{max} = 444 and 406 nm, respectively) afforded resonance-enhanced Raman features (Figure 9). The obvious overall similarity of the data for both compounds corroborates the X-ray crystallographic results, indicating near identity of their structures. Two of the features in the resonance Raman spectra at 1238 and ∼875 cm^{-1} shifted upon $^{15}NO_2^-$ substitution. As described above, this finding, in conjunction with observation of decreased resonance enhancement of these vibrations relative to a sulfate standard as the excitation wavelength was increased from 457 to 613 nm, lends important support for assignment of the absorption bands for the complexes as $Cu^I \rightarrow NO_2^-$ MLCT transitions. The largest isotope shifts occurred for the 1238 cm^{-1} peaks ($\Delta^{15}N/^{14}N$ = 20 and 24 cm^{-1}, respectively, for the Cu^ICu^{II} and Cu^IZn^{II} compounds), the magnitudes of which argue for their assignment as NO_2^- ν_s (typical $\Delta^{15}N/^{14}N$ values for nitro ν_s are ∼20 cm^{-1}).[48] This band also was identified in the IR spectrum of the dicopper(I,II) complex (1235 cm^{-1}; $\Delta^{15}N/^{14}N$ = 21 cm^{-1}). The frequencies and much less pronounced isotope shifts for the sharp 876 cm^{-1} (Cu^ICu^{II}; $\Delta^{15}N/^{14}N$ = 2 cm^{-1}) and 872 cm^{-1} (Cu^IZn^{II}; $\Delta^{15}N/^{14}N$ = 4 cm^{-1}) bands are consistent with their assignment as deformation modes (δ_s); in other nitro complexes, these typically occur at ∼830 cm^{-1} with $\Delta^{15}N/^{14}N$ = 4−5 cm^{-1}.[33,48] Finally, a third distinctive feature is apparent in the resonance Raman spectra, a broad peak at low energy [422 cm^{-1} (Cu^ICu^{II}) and 430 cm^{-1} (Cu^IZn^{II})] which did not appear to shift upon $^{15}NO_2^-$ substitution. This feature may be attributed either to a $Cu^I-N_{nitrite}$ vibration (typical M−N for nitro complexes occur at 300−400 cm^{-1} with $\Delta^{15}N/^{14}N$ = 4 cm^{-1})[33,48] or to a symmetric vibration of the three-atom M^{II}−*O*,*O*-nitrito unit (M^{II} = Cu^{II} or Zn^{II}), which would be expected to have the observed minimal ^{15}N isotope sensitivity but distinct M^{II} dependence. We cannot distinguish between these possibilities at this point in our studies, however.

Electrochemistry. Cyclic voltammetry experiments revealed that $[LCu(CH_3CN)]PF_6$ ($L = L^{i\text{-}Pr_3}$ and L^{Bn_3}) in CH_3CN with 0.5 M $(Bu_4N)(PF_6)$ undergoes electrochemically quasi-reversible [ΔE_p (0.1 V/s) = 110 mV ($L^{i\text{-}Pr_3}$) and 310 mV (L^{Bn_3})] and chemically reversible ($i_{pc} \approx i_{pa}$) one-electron (verified by coulometry) redox transformations with $E_{1/2}$ = 0.36 V ($L^{i\text{-}Pr_3}$) and 0.42 V (L^{Bn_3}) vs SCE. The more positive redox potential for the latter couple (indicative of relatively greater stabilization of the reduced compared to the oxidized state in the former) is consistent with the respective electronic influences of the supporting ligand substituents (Bn is more electron withdrawing than *i*-Pr).[49] Both potentials are less than those measured for analogous $Tp^{RR'}Cu(CH_3CN)$ complexes,[23] presumably because the sp^3 amine donors in the triazacyclononane complexes favor the Cu^{II} state more than the sp^2 pyrazolyl donors in the $Tp^{RR'}$

(48) Cleare, M. J.; Griffith, W. P. *J. Chem. Soc.* **1967**, 1144−1147.

Scheme 2

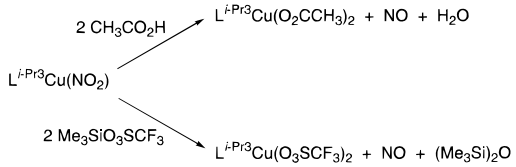

compounds, and in spite of the overall 1+ charge for the former. Divergent propensities of the triazacyclononane and $Tp^{RR'}$ ligands to support nontetrahedral metal ion geometries may also be responsible for the redox potential differences, i.e., the $Tp^{RR'}$ ligands are arguably greater "tetrahedral enforcers",[22] especially when the 3-pyrazolyl substituents are large, and thus drive the redox potential to a higher value because of their tendency to favor geometries suitable for copper(I).

Differences in electrochemical behavior arising from *i*-Pr versus Bn substitution also were observed in cyclic voltammograms of the dicopper(I,I) complexes $[(LCu)_2(\mu\text{-}NO_2)]PF_6$. As already mentioned above, for $L = L^{i\text{-}Pr_3}$, the complex undergoes an electrochemically quasi-reversible [ΔE_p (0.1 V/s) = 110 mV] and chemically reversible ($i_{pa}/i_{pc} \approx 1$) one-electron oxidation with $E_{1/2} = 0.07$ V vs SCE (0.1 M TBAP in CH_2Cl_2), which is associated with a shift in the coordination mode of the bound nitrite ion and the generation of a stable mixed valent, dicopper(I,II) complex. In contrast, $[(L^{Bn_3}Cu)_2(\mu\text{-}NO_2)PF_6$ does not exhibit such clean electrochemical behavior; it is irreversibly oxidized at $E_{pa} = +0.41$ V vs SCE. We currently do not understand why our efforts to generate a stable mixed valence species supported by L^{Bn_3} either electrochemically or chemically have not met with success; clearly, these and other observations[31] demonstrate that differences in the steric and/or electronic properties of $L^{i\text{-}Pr_3}$ and L^{Bn_3} significantly affect the stability and reactivity of their respective copper complexes.

Reactivity: NO Generation. An investigation of the reactivity of $L^{i\text{-}Pr_3}Cu(NO_2)$ with proton sources was undertaken in order to probe the viability of the complex as a functional NiR model, our primary objectives being to observe NO generation and intermediates along the pathway thereto. Decomposition of $(Bu_4N)(NO_2)$ by a mixture of a dicopper(I) complex and $HPF_6{\cdot}Et_2O$ has been reported, but instead of evolving NO, a dicopper(II)−nitrosyl complex formulated as having a $Cu^{II}-(\mu\text{-}NO^-)-Cu^{II}$ core was generated.[16b] Clean evolution of 1 equiv of NO and, presumably, H_2O was observed (GC) when a solution of $L^{i\text{-}Pr_3}Cu(NO_2)$ in CH_2Cl_2 was treated with 2 equiv of glacial acetic acid (Scheme 2). Nitric oxide gas production was accompanied by the quantitative formation of blue $L^{i\text{-}Pr_3}Cu(O_2CCH_3)_2$, which was identified by comparison of its UV−vis and EPR spectra with those of independently synthesized material (*vide infra*). Presumably, the reaction proceeds via nitrite protonation and dehydration to afford a $[CuNO]^{10}$ intermediate ($Cu^I-NO^+ \leftrightarrow Cu^{II}-NO$, in valence bond terms); subsequent ejection of NO from this intermediate and coordination of acetate to the resulting Cu^{II} fragment (not necessarily in that order) would account for the observed final products. We were not able to observe any intermediates in this instance, even when HOAc was added to $L^{i\text{-}Pr_3}Cu(NO_2)$ at −80 °C, suggesting that the latter steps (NO evolution/Cu^{II} trapping) were efficient with the acetate anion. Thus, several other protonic acids or analogs with poorly ligating conjugate bases were screened for their ability to stabilize the postulated nitrosyl intermediate.

Addition of excess $HBF_4{\cdot}Et_2O$ to a solution of $L^{i\text{-}Pr_3}Cu(NO_2)$ at −80 °C initially yielded a promising red solution, but the red color bleached within seconds even at low temperature, with concomitant evolution of both NO (65%) and a small amount of N_2O (<5%). When $Me_3SiO_3SCF_3$ (a "proton acid equivalent") was used instead, the red solution persisted for ca. 5−10 min at −80 °C before turning green and evolving NO and, in this instance, $(Me_3Si)_2O$, allowing acquisition of UV−vis and EPR spectroscopic data. Unfortunately, rather than indicating the presence of a nitrosyl intermediate, these data matched those for the mixed valent cation $[(L^{i\text{-}Pr_3}Cu)_2(\mu\text{-}NO_2)]^{2+}$. We suggest that this compound is formed in a side reaction of $L^{i\text{-}Pr_3}Cu(NO_2)$ starting material and the $L^{i\text{-}Pr_3}Cu^{II}$ fragment resulting from NO loss and that the dicopper(I,II) complex also reacts with H^+ or Me_3Si^+ to afford the observed final products (Scheme 3). In support of these postulates, $[(L^{i\text{-}Pr_3}Cu)_2(\mu\text{-}NO_2)](O_3SCF_3)_2$, which exhibits spectroscopic properties in CH_2Cl_2 identical to those of the red reaction solution, was successfully prepared independently from $L^{i\text{-}Pr_3}Cu(NO_2)$ and $L^{i\text{-}Pr_3}Cu(O_3SCF_3)_2$ and was found to yield NO (68%) and $L^{i\text{-}Pr_3}Cu(O_3SCF_3)_2$ upon treatment with $Me_3SiO_3SCF_3$. Thus, as outlined in Scheme 3, the $L^{i\text{-}Pr_3}Cu^{II}$ fragment resulting from nitrite dehydration and NO loss from $L^{i\text{-}Pr_3}Cu(NO_2)$ appears to undergo competitive trapping by either starting material or the conjugate base of the acid reagent; in the case of HOAc, the latter predominates, preventing observation of the mixed valent species, whereas for $Me_3SiO_3SCF_3$, this species forms at low temperature and persists for sufficient time prior to its decomposition to NO to be spectroscopically identified.

Scheme 3

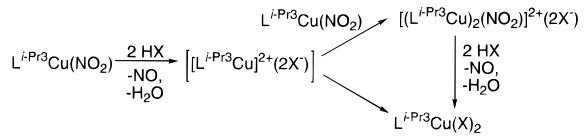

Biological Relevance. The complexes described herein represent the first examples of discrete copper(I)−nitrite adducts to be identified; thus, they provide important precedents for nitrite binding to reduced copper sites in proteins. Such binding is most significant in the catalytic cycle of nitrite reductase, which has been postulated to coordinate NO_2^- at Cu-II (Figure 1). The pseudotetrahedral geometries of the copper(I) ions in the mono- and dinuclear nitrite complexes supported by the hindered triazacyclononane ligands mimic possible topologies for the reduced, tris(histidyl)-ligated Cu-II site. Our observation of both *O*- and *N*-NO_2^- coordination to Cu^I in the synthetic analogs renders either mode a viable option in the biological system. Not surprisingly considering the well-known soft, strong-field nature of the nitrite ion when utilizing its N atom to bind to transition metals,[33] the latter "nitro" mode appears to be thermodynamically favored in the copper(I) complexes. The preferential oxidation of the *O*-bound site to yield a localized mixed valent species that retains the $Cu^I-N\text{-}NO_2^-$ unit can be construed as support for its stability. This argument, in conjunction with the demonstration of quantitative NO evolution upon addition of 2 equiv of protons to $L^{i\text{-}Pr_3}Cu(NO_2)$, provides a basis for suggesting that the substrate adduct having *N*-NO_2^- coordination is the most important enzyme intermediate. Clean dehydration of *O*- or *O*,*O*-bound nitrite in a Cu^{II} complex has not been reported,[18] making such a species a less likely candidate for the direct precursor of NO. Linkage isomerism (*O*-to-*N*-NO_2^-) was observed in a copper(II) system that promoted nitrite reduction when reduced electrochemically.[18c,d] Thus, reduction of an initially formed $Cu^{II}-NO_2^-$ moiety with concomitant isomerization to a $Cu^I-N\text{-}NO_2^-$ intermediate that subsequently generates NO is a reasonable possibility. Presumably, $L^{i\text{-}Pr_3}Cu(NO_2)$ and its enzyme congener evolve NO via a $[CuNO]^{10}$

(49) The carbonyl stretching frequencies in IR spectra of $[LCu(CO)]^+$ (2088 cm^{-1} for $L = L^{Bn_3}$ vs 2067 cm^{-1} for $L = L^{i\text{-}Pr_3}$) corroborate the suggested order of electron-withdrawing capability $L^{Bn_3} > L^{i\text{-}Pr_3}$ (Halfen, J. A.; Mahapatra, S.; Tolman, W. B. Unpublished results).

intermediate, which to date remains an elusive synthetic target and an unsubstantiated metalloprotein moiety. Such a unit has been proposed to form upon reaction of various copper(II)-containing proteins and complexes with NO (see references cited in 17a), but supporting evidence beyond reversible bleaching of Cu^{II}-associated UV−vis and EPR features is lacking in most instances and the only well-characterized mononuclear copper nitrosyl has a [CuNO][11] electron inventory (it is generated upon treatment of a Cu^{I} precursor with NO).[17]

There are many analogies between iron- and copper-containing dissimilatory nitrite reductases with regard to proposed mechanisms and relevant synthetic model complexes. For both, it is believed that nitrite binds to the reduced metal ion (Fe^{II} or Cu^{I}) and undergoes dehydration to an unstable, electrophilic nitrosyl ([FeNO][6] or [CuNO][10]) that subsequently evolves NO and provides the oxidized metal (Fe^{III} or Cu^{II}).[14] Like the compounds we have characterized, an iron(II) porphyrin synthetic model of the protein substrate adduct exhibits nitro coordination characterized by a short $Fe-N_{nitrite}$ bond that gives rise to distinct spectroscopic behavior.[35] Both iron and copper nitrosyls proposed to form upon protonation of the nitrite complexes are less stable than their one-electron reduced counterparts ([FeNO][7] or [CuNO][11]), although in contrast to the case for copper, synthetic porphyrin− and corrole−iron nitrosyls at both oxidation levels have been well-characterized.[50]

A second type of copper protein nitrite adduct is a mixed valent nitritohemocyanin (halfmetNO_2Hc) that has been extensively studied because of the potential for insight into the factors that control dioxygen binding and/or activation in this and related proteins such as tyrosinase.[20] The nitrite-bridged Cu^{I}-Cu^{II} complexes we have described represent possible models of this adduct. Despite some recent controversy,[20g] it has become evident that the initial report by Himmelwright et al.[20d] that nitrite is tightly bound to the active site of halfmetNO_2Hc is correct.[20h] Recent spectroscopic studies on halfmetNO_2Hc[20h] and a mononuclear Cu^{II} form of Hc both with and without bound nitrite[20i] have been interpreted to indicate that nitrite coordinates via an O atom to a single Cu^{II} ion ligated to three histidine residues in a distorted tetragonal geometry. Because of similarities in EPR and ESEEM spectroscopic properties between the mononuclear Cu^{II} Hc and halfmetNO_2Hc and the fact that the latter is completely valence localized, the presence of an additional interaction of nitrite with the second Cu^{I} ion has been questioned.[20h,i] Our discovery of a nitrite-bridged $Cu^{I}Cu^{II}$ compound that also is valence localized and that exhibits an EPR signal typical for a mononuclear Cu^{II} site implies that interaction of nitrite with a Cu^{I} ion may be feasible in the protein. However, this idea is mitigated by the distinct differences between the UV−vis and EPR properties of $[(L^{i\text{-}Pr_3}Cu)_2(\mu\text{-}NO_2)]^{2+}$ and halfmetNO_2Hc, particularly the lack of the MLCT band in the absorption spectrum of the latter, that argue against congruent structures for their dimetal cores.

In sum, the work described herein provides direct experimental support for the viability of $Cu^{I}-NO_2^-$ adducts in biological denitrification processes. Demonstration of their competence to evolve nitric oxide upon protonation further corroborates their suggested significance as intermediates in dissimilatory nitrite reduction by copper proteins. Several issues remain unresolved, however, such as the mechanism of N_2O production[6] and the intermediacy of [CuNO][10] species;[15a] these are the focus of ongoing efforts in our laboratory.

(50) (a) Autret, M.; Will, S.; Caemelbecke, E. V.; Lex, J.; Gisselbrecht, J.-P.; Gross, M.; Vogel, E.; Kadish, K. M. *J. Am. Chem. Soc.* **1994**, *116*, 9141−9149 and references cited therein. (b) Ozawa, S.; Sakamoto, E.; Ichikawa, T.; Watanabe, Y.; Morishima, I. *Inorg. Chem.* **1995**, *34*, 6362−6370.

Experimental Section

General Procedures. All reagents and solvents were obtained from commercial sources and used as received unless otherwise noted. Solvents were dried according to published procedures[51] and distilled under N_2 immediately prior to use. All air-sensitive reactions were performed either in a Vacuum Atmospheres inert atmosphere glovebox under a N_2 atmosphere or by using standard Schlenk and vacuum line techniques. The ligands $L^{i\text{-}Pr_3}$ and L^{Bn_3} were synthesized according to the published procedures.[24,25] Although a variety of syntheses of the parent macrocycle 1,4,7-triazacyclononane have appeared in the literature, we have found that the following methods for the preparation of synthetic intermediates are most efficient. Ethylene glycol ditosylate and diethylenetriamine tris(tosylate) were prepared according to the methods of Ouchi et al.[52] and Verkade et al.,[53] respectively, and both were recrystallized from CH_3CN. The closure of the macrocyclic ring and the subsequent acidic hydrolysis of the product tris(tosylate) were performed according to the method of Searle and Geue.[54] The tris(hydrochloride) salt of 1,4,7-triazacyclononane was isolated by *cautious* addition of 6 M HCl to the sulfuric acid detosylation mixture, followed by precipitation with Et_2O. Isolation of the 1,4,7-triazacyclononane free base was accomplished following the method of Verkade et al.[53] The salts $[Cu(CH_3CN)_4]PF_6$[55] and $Na[B(3,5\text{-}(CF_3)_2C_6H_3)_4]$[30] were prepared as described in the literature. Gas chromatography experiments were performed by using a Hewlett-Packard 5890 Series II gas chromatograph with a HP 3396 Series II integrator, Porpak Q column (6 ft, 20 mL/min flow rate, 30 °C, helium carrier gas), and TCD detector. NO quantitation was performed by calibrating detector response with known concentrations of NO mixed with N_2; molar quantities were calculated using the ideal gas equation. Electrochemical experiments were performed using an EG & G Princeton Applied Research (PAR) VeraStat potentiostat driven by EG & G PAR Model 250 software. The cell used was described previously.[23] Measurements were conducted under an Ar atmosphere, using tetrabutylammonium hexafluorophosphate (TBAP) as the supporting electrolyte. Conductance measurements were made using a YSI Model 35 cnductance meter and analyzed according to a published protocol.[56] IR spectra were recorded on a Perkin Elmer 1600 Series FTIR spectrophotometer as KBr pellets. Resonance Raman spectra were collected on a Spex 1403 spectrometer interfaced with a DM3000 data collection system using Spectra-Physics Models 2030-15 argon ion and 375B CW dye (Rhodamine 6G) lasers. Spectra were obtained at room temperature as KBr pellets, and Raman frequencies are referenced to internal Na_2SO_4 [$\nu_1(SO_4^{2-}) = 998\ cm^{-1}$]. Electronic absorption spectra were recorded on a Hewlett-Packard HP8452A spectrophotometer (190−820 nm scan range) interfaced with a microcomputer for data acquistion and analysis, with low-temperature data collected by using a custom manufactured vacuum Dewar with quartz windows. NMR spectra were recorded on Varian VXR-300 or VXR-500 spectrometers; ^1H and $^{13}C\{^1H\}$ chemical shifts are reported versus tetramethylsilane and referenced to the residual solvent peak(s). $^{31}P\{^1H\}$ NMR spectra are referenced to external 85% H_3PO_4. X-band EPR spectra were recorded on a Bruker ESP300 spectrometer fitted with a liquid nitrogen finger dewar (77 K, ∼9.44 GHz). Fast atom bombardment (FAB) mass spectra were determined using a VG 7070E-HF mass spectrometer with xenon gas for ionization. Electrospray ionization mass spectral data were collected using a Sciex API III mass spectrometer, with scanning performed in 0.2 Da steps and a 5−10 ms dwell time per step. Signal averaging was used to enhance the signal-to-noise ratio. Elemental analyses were performed by Atlantic Microlabs of Norcross, GA.

$[L^{i\text{-}Pr_3}Cu(CH_3CN)]PF_6$. To a solution of $L^{i\text{-}Pr_3}$ (0.421 g, 1.65 mmol) in THF (5 mL) was added $[Cu(CH_3CN)_4]PF_6$ (0.611 g, 1.64 mmol) as a solid. The resultant mixture was stirred for 1 h and then filtered to remove any remaining solid. Pentane (10 mL) was then added to the

(51) Perrin, D. D.; Armarego, W. L. F. *Purification of Laboratory Chemicals*; Pergamon Press: New York, 1988.

(52) Ouchi, M.; Inoue, Y.; Liu, Y.; Nagamune, S.; Nakamura, S.; Wada, K.; Hakushi, T. *Bull. Chem. Soc. Jpn.* **1990**, *63*, 1260−1262.

(53) White, D. W.; Karcher, B. A.; Jacobsen, R. A.; Verkade, J. G. *J. Am. Chem. Soc.* **1979**, *101*, 4921−4925.

(54) Searle, G. H.; Geue, R. J. *Aust. J. Chem.* **1984**, *37*, 959−970.

(55) Kubas, G. J. *Inorg. Synth.* **1979**, *19*, 90−92; **1990**, *28*, 68−70.

(56) Geary, W. J. *Coord. Chem. Rev.* **1971**, *7*, 81.

nearly colorless filtrate with rapid stirring, causing the precipitation of the product as a white powder (0.655 g, 80%): mp 124 °C dec; ^{1}H NMR (CD_2Cl_2, 500 MHz) δ 3.05 (septet, J = 6.5 Hz, 3H), 2.79−2.72 (m, 6H), 2.48−2.42 (m, 6H), 1.94 (s, 3H), 1.20 (d, J = 6.5 Hz, 18H) ppm; ^{13}C{^{1}H} NMR (CD_2Cl_2, 125 MHz): δ 164.6, 58.55, 51.2, 20.0, 3.2 ppm; FTIR (KBr, cm^{-1}) 2974, 2935, 2854, 2267 (C≡N), 1496, 1471, 1452, 1386, 1367, 1350, 1324, 1296, 1278, 1164, 1128, 1072, 1050, 967, 955, 877, 840 (PF_6^-), 779, 759, 719, 556 (PF_6^-); FAB-MS (MNBA) *m/e* (relative intensity) 359 ([M − PF_6]$^+$, 15), 318 ([M − CH_3CN − PF_6]$^+$, 100). Anal. Calcd for $C_{17}H_{36}CuF_6N_4P$: C, 40.43; H, 7.19; N, 11.09. Found: C, 40.72; H, 6.95; N, 11.23.

[L^{Bn_3}Cu(CH_3CN)]PF_6. To a solution of L^{Bn_3} (0.330 g, 0.83 mmol) in THF (10 mL) was added [Cu(CH_3CN)$_4$]PF_6 (0.308 g, 0.83 mmol). The resultant mixture was stirred for 1 h and then filtered to remove any remaining solid. Heptane (20 mL) was added to the yellow filtrate with rapid stirring, causing the formation of an oil. Upon treatment of this oil with MeOH, the product was obtained as a light tan solid (0.33 g, 62%): ^{1}H NMR (CD_2Cl_2, 300 MHz) δ 7.34−7.30 (m, 15H), 3.82 (s, 6H), 2.72−2.62 (m, 6H), 2.55−2.45 (m, 6H), 2.35 (s, 3H) ppm; ^{13}C{^{1}H} NMR (CD_2Cl_2, 75 MHz): δ 141.21, 135.10, 131.2, 128.8, 117.4, 64.3, 52.4, 0.4 ppm; FTIR (KBr, cm^{-1}) 3087, 3059, 3028, 2973, 2935, 2854, 2267 (C≡N), 1495, 1471, 1386, 1367, 1277, 1164, 1137, 1128, 1071, 1049, 967, 955, 876, 837 (PF_6^-), 759, 719 cm^{-1}; FAB-MS (MNBA) *m/e* (relative intensity) 462 ([M − CH_3CN − PF_6]$^+$, 100). Anal. Calcd for $C_{29}H_{36}CuF_6N_4P$: C, 53.69; H, 5.60; N, 8.64. Found: C, 53.51; H, 5.54; N, 8.69.

[(L$^{i\text{-}Pr_3}$Cu)$_2$(μ-NO_2)]PF_6. To a solution of [L$^{i\text{-}Pr_3}$Cu(CH_3CN)]PF_6 (0.145 g, 0.287 mmol) in MeOH (10 mL) was added $NaNO_2$ (0.140 g, 2.03 mmol) dissolved in MeOH (5 mL). The solution immediately turned yellow, and a small amount of a dark solid precipitated. After stirring for 15 min, the solvent was removed under vacuum, leaving an orange residue. This residue was extracted with CH_2Cl_2 (15 mL), the extracts were filtered, and the solvent was removed from the filtrate to afford an orange solid. Crystallization from THF/pentane yielded pure product as yellow-orange plates suitable for X-ray crystallographic analysis (0.106 g, 89%): mp 178 °C dec; ^{1}H NMR (CD_2Cl_2, 300 MHz) δ 3.13 (m, 6H), 2.86−2.79 (m, 12H), 2.56−2.49 (m, 12H), 1.17 (d, J = 6.3 Hz, 36H) ppm; ^{13}C{^{1}H} NMR (CD_2Cl_2, 75 MHz) δ 58.0, 51.0, 19.7 ppm; FTIR (KBr, cm^{-1}) 2967, 1492, 1466, 1388, 1364, 1352 (1333 $^{15}NO_2^-$), 1279, 1262, 1185 (1168 $^{15}NO_2^-$), 1151, 1124, 1078, 1050, 1018, 966, 841 (PF_6^-), 749, 715, 663, 598, 557 (PF_6^-); FAB-MS (MNBA) *m/e* (relative intensity) 682 ([M − PF_6]$^+$, 20), 318 ([M − L$^{i\text{-}Pr_3}$Cu − NO_2 − PF_6]$^+$, 100). Anal. Calcd for $C_{30}H_{66}Cu_2F_6N_7O_2P$: C, 43.47; H, 8.03; N, 11.83. Found: C, 43.57; H, 7.98; N, 11.81.

[(L^{Bn_3}Cu)$_2$(μ-NO_2)]PF_6. A procedure identical to that for the synthesis of [(L$^{i\text{-}Pr_3}$Cu)$_2$(μ-NO_2)]PF_6 was followed, except [L^{Bn_3}Cu(CH_3-CN)]PF_6 (0.234 g, 0.36 mmol) was used as the starting material. This precursor is insoluble in MeOH, but upon addition of the solution of $NaNO_2$, it dissolved and the reaction and workup proceeded as for the L$^{i\text{-}Pr_3}$ analog. The product was isolated as yellow-orange needles from CH_2Cl_2/Et_2O (0.178 g, 89%): ^{1}H NMR (acetone-d_6, 300 MHz) δ 7.57−7.55 (m, 6H), 7.26−7.24 (m, 9H), 4.02 (s, 6H), 2.83−2.67 (m, 6H), 2.73−2.66 (m, 6H) ppm; ^{13}C{^{1}H} NMR (acetone-d_6, 75 MHz) δ 136.5, 131.7, 129.0, 128.7, 64.2, 52.6 ppm; FTIR (KBr, cm^{-1}) 3087, 3059, 3028, 2998, 2969, 2928, 2775, 1496, 1453, 1347 (1331 $^{15}NO_2^-$), 1332, 1287, 1202 (1174 $^{15}NO_2^-$), 1127, 1104, 1093, 1075, 1060, 1002, 987, 924, 896, 872, 835 (PF_6^-), 786, 764, 731, 710, 702, 695. Anal. Calcd for $C_{54}H_{66}Cu_2F_6N_7O_2P$: C, 58.05; H, 5.95; N, 8.78. Found: C, 57.40; H, 5.87; N, 8.72.

[(L$^{i\text{-}Pr_3}$Cu)$_2$(μ-NO_2)](PF_6)$_2$. To a solution of [(L$^{i\text{-}Pr_3}$Cu)$_2$(μ-NO_2)]PF_6 (0.158 g, 0.190 mmol) in CH_2Cl_2 (5 mL) was added ferricenium hexafluorophosphate (Cp_2Fe)PF_6, 0.063 g, 0.190 mmol). As the oxidizing agent slowly dissolved, the color of the solution changed from orange to deep red. After 30 min of stirring, Et_2O (10 mL) was added, causing the precipitation of a brown powder, which was recrystallized from CH_2Cl_2/Et_2O to yield the product as nearly black cubes (0.140 g, 76%): mp 192 °C dec; FTIR (KBr, cm^{-1}) 2978, 1491, 1474, 1389, 1351, 1235 (1214 $^{15}NO_2^-$), 1170, 1070, 965, 838 (PF_6^-), 757, 720, 669, 557 (PF_6^-). Anal. Calcd for $C_{30}H_{66}Cu_2F_{12}N_7O_2P_2$: C, 36.00; H, 6.83; N, 10.07. Found: C, 36.23; H, 6.72; N, 9.67.

[(L$^{i\text{-}Pr_3}$Cu)$_2$(μ-NO_2)][B(3,5-(CF_3)$_2$$C_6H_3$)$_4$]$_2$. A solution of [(L$^{i\text{-}Pr_3}$-Cu)$_2$($NO_2$)]($PF_6$)$_2$ (0.045 g, 0.046 mmol) in CH_2Cl_2 (5 mL) was treated with a solution of Na[B(3,5-(CF_3)$_2$$C_6H_3$)$_4$] (0.082 g, 0.092 mmol) in Et_2O (2 mL), causing the deposition of a white powder. After standing for 1 h at −20 °C, the mixture was filtered; storage of the filtrate at −20 °C overnight produced small dark crystals of [(L$^{i\text{-}Pr_3}$)$_2$$Cu_2$($NO_2$)]-[B(3,5-($CF_3$)$_2$$C_6H_3$)$_4$]$_2$ (0.105 g, 96%). Crystallization from CH_2Cl_2/toluene produced crystals suitable for X-ray diffraction: FTIR (KBr, cm^{-1}) 2986, 2946, 2877, 1607, 1471, 1355, 1282, 1227, 1186, 1156, 1122, 960, 887, 837, 714, 683, 667. Anal. Calcd for $C_{94}H_{90}$-$Cu_2B_2F_{48}N_7O_2$: C, 46.84; H, 3.76; N, 4.07. Found: C, 46.73; H, 3.75; N, 4.10.

[L$^{i\text{-}Pr_3}$Cu(PPh_3)]PF_6. To a solution of [L$^{i\text{-}Pr_3}$Cu(CH_3CN)]PF_6 (0.123 g, 0.244 mmol) in THF (5 mL) was added PPh_3 (0.064 g, 0.246 mmol). A fine white solid precipitated almost immediately, which was recrystallized from CH_2Cl_2/Et_2O to yield the product as colorless needles (0.123 g, 70%): mp > 250 °C; ^{1}H NMR (CD_2Cl_2, 300 MHz) δ 7.51−7.40 (m, 9H), 7.28−7.22 (m, 6H), 2.98 (septet, J = 6.6 Hz, 3H), 2.88−2.78 (m, 6H), 2.75−2.65 (m, 6H), 0.98 (d, J = 6.6 Hz, 18H) ppm; ^{13}C{^{1}H} NMR (CD_2Cl_2, 75 MHz) δ 133.3, 133.1, 131.0, 129.3, 129.4, 59.5, 36.5, 18.9 ppm; ^{31}P{^{1}H} NMR (CD_2Cl_2, 121 MHz) δ 5.27 ppm; FTIR (KBr, cm^{-1}) 3053, 2987, 2937, 2869, 1491, 1479, 1466, 1434, 1388, 1366, 1351, 1328, 1299, 1281, 1265, 1163, 1127, 1092, 1068, 1023, 99i, 965, 877, 838 (PF_6^-), 787, 756, 744, 719, 696, 585, 556 (PF_6^-), 531; FAB-MS (MNBA) *m/e* (relative intensity) 580 ([M − PF_6]$^+$, 100). Anal. Calcd for $C_{33}H_{48}CuF_6N_3P_2$: C, 54.58; H, 6.66; N, 5.79. Found: C, 55.27; H, 6.80; N, 5.88.

L$^{i\text{-}Pr_3}$Cu(NO_2). To a solution of [(L$^{i\text{-}Pr_3}$Cu)$_2$(μ-NO_2)]PF_6 (0.222 g, 0.27 mmol) in THF (5 mL) was slowly added PPh_3 (0.071 g, 0.27 mmol) dissolved in THF (5 mL). The original orange solution gradually changed to bright yellow, and a white precipitate of [L$^{i\text{-}Pr_3}$Cu(PPh_3)]-PF_6 appeared. After filtering, the filtrate was evaporated to dryness. The resulting yellow powder was dissolved in CH_2Cl_2 (5 mL) and treated with Et_2O (20 mL), causing the precipitation of additional [L$^{i\text{-}Pr_3}$Cu(PPh_3)]PF_6. The mixture was then filtered again, and the filtrate volume was reduced to 3 mL causing the appearance of a small additional amount of the phosphine complex, to give a total yield of 0.190 g (97%). Following a final filtration, the filtrate was evaporated to dryness and the yellow residue was redissolved in a small amount of THF. Diffusion of pentane into this THF solution resulted in the crystallization of L$^{i\text{-}Pr_3}$Cu(NO_2) as yellow plates (0.062 g, 63%): mp 147 °C dec; ^{1}H NMR (CD_2Cl_2, 300 MHz) δ 3.24 (septet, J = 6.9 Hz, 3H), 2.88−2.81 (m, 6H), 2.52−2.45 (m, 6H), 1.25 (d, J = 6.9 Hz, 18H) ppm; ^{13}C{^{1}H} NMR (CD_2Cl_2, 75 MHz) δ 57.8, 50.6, 19.2 ppm; FTIR (KBr, cm^{-1}) 2968, 2887, 2841, 1493, 1485, 1470, 1453, 1386, 1370, 1344, 1324, 1306 (1258 $^{15}NO_2^-$), 1268 (1247 $^{15}NO_2^-$), 1169, 1124, 1068, 1047, 1015, 963, 801, 755, 717, 583; FAB-MS (MNBA) *m/e* (relative intensity) 364 ([M]$^+$, 5), 318 ([M − NO_2]$^+$, 100). Anal. Calcd for $C_{15}H_{33}CuN_4O_2$: C, 49.36; H, 9.11; N, 15.35. Found: C, 48.95; H, 8.96; N, 14.69.

[L$^{i\text{-}Pr_3}$Cu(μ-NO_2)ZnL$^{i\text{-}Pr_3}$](O_3SCF_3)$_2$. Solid Zn(O_3SCF_3)$_2$ (0.091 g, 0.25 mmol) as added to a solution of L$^{i\text{-}Pr_3}$ (0.064 g, 0.25 mmol) in CH_2Cl_2 (8 mL). After allowing the slurry to stir for 1 h, a solution of L$^{i\text{-}Pr_3}$Cu(NO_2) (0.046 g, 0.126 mmol) in CH_2Cl_2 (2 mL) was added a deep red color gradually developed. The solution was stirred overnight and filtered, and Et_2O was diffused into the filtrate to yield the product as red crystals (0.095 g, 76%): ^{1}H NMR (CD_2Cl_2, 500 MHz) δ 3.27−3.20 (m, 6H), 3.04 (s, 12H), 2.91−2.86 (m, 6H), 2.67−2.62 (m, 6H), 1.22 (d, J = 6.5 Hz, 18H), 1.18 (d, J = 7.0 Hz, 18H); ^{13}C NMR (CD_2-Cl_2, MHz) δ 58.6, 57.5, 51.3, 49.3, 19.8, 18.8 ppm; FTIR (KBr, cm^{-1}) 2980, 2939, 1492, 1470, 1393, 1377, 1263 ($O_3SCF_3^-$), 1222, 1149 ($O_3SCF_3^-$), 1029 ($O_3SCF_3^-$), 639 ($O_3SCF_3^-$), 516; ISP-MS *m/e* (relative intensity) 832 ([M − O_3SCF_3]$^+$, 50), 359 (100). Anal. Calcd for $C_{32}H_{66}CuF_6N_7O_8S_2Zn$: C, 39.13; H, 6.78; N, 9.99. Found: C, 39.18; H, 6.82; N, 10.00.

L$^{i\text{-}Pr_3}$Cu(O_2CCH_3)$_2$·H_2O. To a solution of L$^{i\text{-}Pr_3}$ (0.036 g, 0.14 mmol) in MeOH (5 mL) was added solid Cu(O_2CCH_3)$_2$·H_2O (0.0293 g, 0.15 mmol), causing the solution to become bright blue. Removal of solvent followed by crystallization from THF/pentane at −20 °C yielded the product as blue blocks (0.048 g, 77%): mp 112 °C dec; FTIR (KBr, cm^{-1}) 3445 (H_2O), 2973, 1628 [ν(C═O)], 1571, 1501, 1471, 1380, 1320 [ν(C─O)], 1262, 1168, 1148, 1126, 1068, 1054, 1013, 967, 844, 763, 721, 664, 647, 607; Λ_M (CH_3CN) 8(1) cm^2 Ω^{-1} mol^{-1}; FAB-MS (MNBA) *m/e* (relative intensity) 377.2 ([M − OAc]$^+$, 100).

Anal. Calcd for $C_{19}H_{41}CuN_3O_5$: C, 50.15; H, 9.08; N, 9.23. Found: C, 50.16; H, 9.02; N, 9.33. Although a water of hydration was not present in the crystal subjected to crystallographic analysis, the complex is rather hygroscopic and is formulated as a monohydrate on the basis of FTIR and elemental analysis data.

$L^{i\text{-}Pr_3}Cu(O_3SCF_3)_2$ and $[L^{i\text{-}Pr_3}Cu(H_2O)(O_3SCF_3)]O_3SCF_3$. To a solution of $L^{i\text{-}Pr_3}$ (0.192 g, 0.752 mmol) in THF (5 mL) was added solid $Cu(O_3SCF_3)_2$ (0.260 g, 0.72 mmol). After being stirred for 2 h, the mixture was filtered. The filtrate was treated with pentane (10 mL) and stored at −20 °C to yield the product as green microcrystals (0.242 g, 55%): FTIR (KBr, cm^{-1}) 2980, 1501, 1327, 1279 ($O_3SCF_3^-$), 1241 ($O_3SCF_3^-$), 1208 ($O_3SCF_3^-$), 1172 ($O_3SCF_3^-$), 1070, 1027 ($O_3SCF_3^-$), 1024 ($O_3SCF_3^-$), 961, 771, 724, 635 ($O_3SCF_3^-$), 576, 518; Λ_M (CH_2Cl_2), 2(1) $cm^2\ \Omega^{-1}\ mol^{-1}$; Λ_M (acetone) 120(2) $cm^2\ \Omega^{-1}\ mol^{-1}$; Λ_M (CH_3CN) 300(2) $cm^2\ \Omega^{-1}\ mol^{-1}$; FAB-MS (MNBA) *m/e* (relative intensity) 467 ($[M - O_3SCF_3]^+$, 75), 318 ($[M - 2O_3SCF_3]^+$, 100). Anal. Calcd for $C_{17}H_{33}CuF_6N_3O_6S_2$: C, 33.09; H, 5.39; N, 6.81. Found: C, 33.23; H, 5.69; N, 6.90. Crystals suitable for X-ray diffraction were obtained only when using wet solvents. Thus, crystallization by vapor diffusion of Et_2O into a 1:3 (v/v) mixture of acetone (wet)/THF yielded green plates of $[L^{i\text{-}Pr_3}Cu(H_2O)(O_3SCF_3)]O_3SCF_3$, as identified by X-ray crystallography and elemental analysis. Calcd for $C_{17}H_{35}CuF_6N_3O_7S_2$: C, 32.15; H, 5.55; N, 6.62; S, 10.10. Found: C, 32.11; H, 5.36; N, 6.62; S, 10.02.

$[(L^{i\text{-}Pr_3}Cu)_2(\mu\text{-}NO_2)](O_3SCF_3)_2$. To a solution of $L^{i\text{-}Pr_3}Cu(NO_2)$ (0.0062 g, 0.017 mmol) in CH_2Cl_2 (2 mL) was added a solution of $L^{i\text{-}Pr_3}Cu(O_3SCF_3)_2$ (0.0105 g, 0.017 mmol) in CH_2Cl_2 (2 mL). The solution immediately turned deep red. Diffusion of Et_2O directly into this solution caused the crystallization of the product as small dark needles in nearly quantitative yield. This compound exhibited UV−vis and EPR spectra identical to those for the PF_6^- and $[B(3,5\text{-}(CF_3)_2C_6H_3)_4]^-$ salts described above: FTIR (KBr, cm^{-1}) 2977, 2942, 2882, 1493, 1472, 1393, 1373, 1257 ($O_3SCF_3^-$), 1227 ($O_3SCF_3^-$), 1159 ($O_3SCF_3^-$), 1067, 1046, 1028 ($O_3SCF_3^-$), 964, 869, 842, 761, 720, 668, 637 ($O_3SCF_3^-$), 572, 517. Anal. Calcd for $C_{32}H_{66}Cu_2F_6N_7O_8S_2$: C, 39.14; H, 6.77; N, 9.98. Found: C, 39.13; H, 6.64; N, 9.81.

Reaction of $L^{i\text{-}Pr_3}Cu(NO_2)$ with CH_3CO_2H. A solution of $L^{i\text{-}Pr_3}Cu(NO_2)$ (0.0044 g, 0.012 mmol) in CH_2Cl_2 (0.15 mL) was prepared in a small vial capped with a rubber septum. A degassed solution of CH_3CO_2H (1.8 μL) in CH_2Cl_2 (0.05 mL) was then introduced via syringe at room temperature. The solution changed immediately from yellow to blue. Analysis of the head space gas by GC indicated that NO(g) had been generated (0.012 mmol, 100%). The copper-containing product of the reaction was identified as $L^{i\text{-}Pr_3}Cu(O_2CCH_3)_2$ by comparison of UV−vis and EPR spectra of the blue solution to those of independently synthesized material.

Reaction of $L^{i\text{-}Pr_3}Cu(NO_2)$ with $Me_3SiO_3SCF_3$. A procedure identical to that used for the reaction of $L^{i\text{-}Pr_3}Cu(NO_2)$ with CH_3CO_2H (above) was followed. Reaction of $L^{i\text{-}Pr_3}Cu(NO_2)$ (0.0066 g, 0.018 mmol) in CH_2Cl_2 (0.15 mL) with $Me_3SiO_3SCF_3$ (7 μL) in CH_2Cl_2 (0.05 mL) at room temperature caused a color change from yellow to green. GC analysis of the head space gas indicated NO(g) generation (0.013 mmol, 70%). The copper-containing product of the reaction was identified as $L^{i\text{-}Pr_3}Cu(O_3SCF_3)_2$ by comparison of UV−vis and EPR spectra of the green solution to those of independently synthesized material. Upon addition of $Me_3SiO_3SCF_3$ to a solution of $L^{i\text{-}Pr_3}Cu(NO_2)$ in CH_2Cl_2 at −80 °C, a red color developed which ultimately changed to green upon warming; UV−vis data acquired at −80 °C matched those obtained for independently synthesized $[(L^{i\text{-}Pr_3}Cu)_2(\mu\text{-}NO_2)](O_3SCF_3)_2$.

Reaction of $[(L^{i\text{-}Pr_3}Cu)_2(\mu\text{-}NO_2)](O_3SCF_3)_2$ with $Me_3SiO_3SCF_3$. A procedure identical to that described above was followed except using the dinuclear starting material. Reaction of $[(L^{i\text{-}Pr_3}Cu)_2(\mu\text{-}NO_2)](O_3SCF_3)_2$ (0.0061 mg, 0.0062 mmol) in CH_2Cl_2 (0.15 mL) with $Me_3SiO_3SCF_3$ (3 μL) in CH_2Cl_2 (0.05 mL) at room temperature caused a color change from red to green. GC analysis of the head space gas indicated NO(g) generation (0.0042 mmol, 68%). The copper-containing product of the reaction was identified as $L^{i\text{-}Pr_3}Cu(O_3SCF_3)_2$ by comparison of UV−vis and EPR spectra of the green solution to those of independently synthesized material.

X-ray Crystallography. $[(L^{i\text{-}Pr_3}Cu)_2(\mu\text{-}NO_2)][B(3,5\text{-}(CF_3)_2C_6H_3)_4]_2$. An irregularly shaped brown crystal of the complex was mounted on a glass fiber with heavy-weight oil and transferred to the cold stream of an Enraf-Nonius CAD-4 diffractometer with graphite monochromated Mo Kα radiation (λ = 0.710 69 Å). Relevant crystallographic information is given in Table 2. Cell constants were obtained from a least squares refinement of the setting angles for 24 carefully centered reflections in the range $21.00° < 2\theta < 43.00°$. The intensity data were collected using the $\omega-2\theta$ scan technique to a maximum 2θ value of 52.0°. An empirical absorption correction was applied, using the program DIFABS,[57] which resulted in transmission factors ranging from 0.78 to 1.20. The data were corrected for Lorentz and polarization effects; no decay correction was applied.

The structure was solved by direct methods[58] using the TEXSAN software package.[59] Non-hydrogen atoms were refined anisotropically, and the hydrogen atoms were placed at calculated positions. The maximum and minimum peaks on the final difference Fourier map corresponded to 0.65 and −0.54 $e^-/Å^3$, respectively. Neutral-atom scattering factors[60] and anomalous dispersion terms[61] were taken from the literature. Because the apparent space group is $P\bar{1}$, the cation is end-for-end disordered and the Cu−N,O distances are based on average positions of the atoms involved, with the exception of the nitrite atoms (N1, O1, O2), which were located in both disordered positions (but refined isotropically). There is also disorder in one of the isopropyl groups (C13) and three of the CF_3 groups. The isopropyl group occurs in all three possible orientations and was modeled with occupancies for three isopropyl groups of C13−C14−C15 (0.579), C13−C14−C16 (0.149), and C13−C15−C16 (0.272). For the CF_3 groups, occupancies are C117−F111−F112−F113 (0.65)/C119−F117−F118−F119 (0.35), C128−F124−F125−F126 (0.75)/C129−F127−F128−F129 (0.25), and C147−F141−F142−F143 (0.67)/C149−F147−F148−F149 (0.33). The major component in each case was refined anisotropically, and the minor component was treated as a rigid group with individual isotropic displacement parameters. Drawings of the cation appear in Figures 5 and 6, and selected bond lengths and angles are presented in Table 1. Complete structure diagrams and full tables of bond lengths and angles, atomic positional parameters, and final thermal parameters for non-hydrogen atoms are given in the supporting information.

$[L^{i\text{-}Pr_3}Cu(H_2O)(O_3SCF_3)]O_3SCF_3$. A green plate crystal of the complex was mounted on a glass fiber with heavy-weight oil and transferred to the cold stream of the Enraf-Nonius CAD4 diffractometer. Data collection was as described above. Important crystallographic information is given in Table 2. Cell constants were obtained from a least squares refinement of the setting angles for 20 carefully centered reflections in the range $10.00° < 2\theta < 48.00°$. The intensity data were collected using the $\omega-2\theta$ scan technique to a maximum 2θ value of 56.0°. An empirical absorption correction was applied on the basis of azimuthal scans of several reflections, which resulted in transmission factors ranging from 0.72 to 1.00. The data were corrected for Lorentz and polarization effects; no decay correction was applied. A correction for secondary extinction was applied (coefficient = $0.159\ 69 \times 10^{-6}$).

The structure was solved by direct methods[58] using the TEXSAN software package.[59] Non-hydrogen atoms were refined anisotropically, and the hydrogen atoms were placed at calculated positions. A search for hydrogen atoms on the coordinated water molecule (O1) was unsuccessful; no attempt to place such atoms in idealized positions was made. The maximum and minimum peaks on the final difference Fourier map corresponded to 1.10 and −1.27 $e^-/Å^3$, respectively. An ORTEP drawing of the structure appears in Figure 4, and selected bond lengths and angles are presented in Table 1. Full tables of bond lengths and angles, atomic positional parameters, and final thermal parameters for non-hydrogen atoms are given in the supporting information.

$[L^{i\text{-}Pr_3}Cu(\mu\text{-}NO_2)ZnL^{i\text{-}Pr_3}](O_3SCF_3)_2$. A dark red block-shaped crystal of the compound was attached to a glass fiber and mounted on a Siemens SMART system for data collection at 173(2) K. An initial

(57) Walker, N.; Stuart, D. *Acta Crystallogr*. **1983**, *A39*, 158−166.
(58) Calabrese, J. C. PHASE: Patterson Heavy Atom Solution Extractor. Ph.D. Thesis, University of Wisconsin, Madison, WI, 1972.
(59) *TEXSAN-Texray Structure Analysis Package*; Molecular Structure Corp.: The Woodlands, TX, 1985.
(60) Cromer, D. T. *International Tables for X-ray Crystallography*; The Kynoch Press: Birmingham, U.K., 1974; Vol. IV, Table 2.2A.
(61) (a) Ibers, J. A.; Hamilton, W. C. *Acta Crystallogr*. **1964**, *17*, 781. (b) Cromer, D. T. *International Tables for X-ray Crystallography*; The Kynoch Press: Birmingham, U.K., 1974; Vol. IV, Table 2.3.1.

set of cell constants was calculated from reflections harvested from three sets of 30 frames. These initial sets of frames were oriented such that orthogonal wedges of reciprocal space were surveyed, thus producing orientation matrices determined from 196 reflections. Final cell constants were calculated from a set of 8192 strong reflections from the actual data collection. Final cell constants reported in this manner usually are about 1 order of magnitude better in precision than those reported from four-circle diffractometers. The data collection technique used for this specimen is generally known as a hemisphere collection. A randomly oriented region of reciprocal space was surveyed to the extent of 1.3 hemispheres to a resolution of 0.87 Å. Three swaths of frames were collected with 0.30° steps in ω. This collection strategy provides a high degree of redundancy in the data and good ψ input in the event a semiempirical absorption correction is applied; here, a semiempirical correction afforded minimum and maximum transmission factors of 0.624 and 0.871, respectively. See Table 2 for additional crystal and refinement information.

The space group $P2_1/c$ was determined on the basis of systematic absences and intensity statistics, and a successful direct-methods solution was calculated which provided most nonhydrogen atoms from the E map. The metric parameter β is close to 90.0°, but the Lane symmetry was determined to be 2/*m* and not *mmm*. Several full-matrix least squares/difference Fourier cycles were performed which located the remainder of the nonhydrogen atoms, all of which were refined with anisotropic displacement parameters. All hydrogen atoms were placed in ideal positions and refined as riding atoms with individual isotropic displacement parameters. Two isopropyl groups were found to be disordered; these groups are atoms C7, C8, and C9 and C10, C11, and C12, respectively. The requisite atoms were refined such that the occupancy equaled 1.0. C11 and C12 coincidentally appear in the same location in both orientations; C11′ and C12′ are entered in the atom list only to provide proper geometry for the calculation of the associated tertiary riding hydrogen. Drawings of the cation appear in Figures 5 and 6, and selected bond lengths and angles are presented in Table 1. Full details of the structure determination, including tables of bond lengths and angles, atomic positional parameters, and final thermal parameters for non-hydrogen atoms, are given in the supporting information. All calculations were performed using SGI INDY R4400-SC or Pentium computers with the SHELXTL-Plus V5.0 program suite.[62]

Acknowledgment. Funding in support of this research was provided by the National Institutes of Health (GM47365 to W.B.T., a SURE Supplement to A.G., GM33162 to L.Q., and a predoctoral traineeship to E.C.W.), the Searle Scholars Program/Chicago Community Trust, the University of Minnesota Undergraduate Research Opportunities Program (A.G.), and the National Science Foundation (National Young Investigator Award to W.B.T. and CHE-9413114 for partial funding for the purchase of the Siemens SMART system). W.B.T. is a recipient of research fellowships from the Alfred P. Sloan and Camille and Henry Dreyfus Foundations. We thank Professor Doyle Britton for his work on the X-ray structures of $[(L^{i\text{-}Pr_3}Cu)_2(\mu\text{-}NO_2)][B(3,5\text{-}(CF_3)_2C_6H_3)_4]_2$ and $[L^{i\text{-}Pr_3}Cu(H_2O)(O_3SCF_3)]O_3SCF_3$ and Dr. Marilyn M. Olmstead for solving the X-ray structure of $[(L^{i\text{-}Pr_3}Cu)_2(\mu\text{-}NO_2)]PF_6$ (cited in ref 21a).

Supporting Information Available: Complete drawings and full details of the structure determinations, including tables of bond lengths and angles, atomic positional parameters, and final thermal parameters for all atoms for $[(L^{i\text{-}Pr_3}Cu)_2(\mu\text{-}NO_2)][B(3,5\text{-}(CF_3)_2C_6H_3)_4]_2$, $[L^{i\text{-}Pr_3}Cu(H_2O)(O_3SCF_3)]O_3SCF_3$, and $[L^{i\text{-}Pr_3}Cu(\mu\text{-}NO_2)ZnL^{i\text{-}Pr_3}](O_3SCF_3)_2$ (51 pages). This material is contained in many libraries on microfiche, immediately follows this article in the microfilm version of the journal, can be ordered from the ACS, and can be downloaded from the Internet; see any current masthead page for ordering information and Internet access instructions.

JA952691I

(62) SHELXTL-Plus V5.0, Siemens Industrial Automation, Inc., Madison, WI.